VPI - AOE - 210

SENSITIVITY ANALYSIS OF DYNAMIC AEROELASTIC RESPONSES IN TRANSONIC FLOW

Jason Cherian Issac
and
Rakesh K. Kapania

Department of Aerospace Engineering

Report submitted to NASA Langley Research Center on the project "Shape Sensitivity Analysis of Static and Dynamic Aeroelastic Responses" under contract NAG1-1411

SENSITIVITY ANALYSIS OF DYNAMIC AEROELASTIC RESPONSES IN TRANSONIC FLOW

Jason Cherian Issac
Rakesh K. Kapania

Aerospace and Ocean Engineering

ABSTRACT

Flutter analysis of a two degree of freedom airfoil in compressible flow is performed using a state-space representation of the unsteady aerodynamic behavior. Indicial response functions are used to represent the normal force and moment response of the airfoil. The structural equations of motion of the airfoil with bending and torsional degrees of freedom are coupled to the unsteady airloads and the aeroelastic system so modelled is solved as an eigenvalue problem to determine the stability. The aeroelastic equations are also directly integrated with respect to time and the time-domain results compared with the results from the eigenanalysis. A good agreement is obtained. The derivatives of the flutter speed obtained from the eigenanalysis are calculated with respect to the mass and stiffness parameters by both analytical and finite-difference methods for various transonic Mach numbers. The experience gained from the two degree of freedom model is applied to study the sensitivity of the flutter response of a wing with respect to various shape parameters. The parameters being considered are: (i) aspect ratio, (ii) surface area of the wing, (iii) taper ratio and (iv) sweep. The wing deflections are represented by Chebyshev polynomials. The compressible aerodynamic state-space model used for the airfoil section is extended to represent the unsteady aerodynamic forces on a generally laminated tapered skewed wing. The aeroelastic equations are solved as an eigenvalue problem to determine the flutter speed of the wing. The derivatives of the flutter speed with respect to the shape parameters are calculated by both analytical and finite difference methods.

ACKNOWLEDGEMENT

The work presented here is a part of the work done in the project sponsored by NASA, Langley Research Center under contract NAG-1-1411 to VPI&SU. We are thankful to Dr. J-F.M. Barthelemy, NASA Langley, for the fruitful discussions we have had with him and the valuable suggestions offered.

TABLE OF CONTENTS

1. INTRODUCTION

Flutter is a dynamic aeroelastic instability that involves the coupling of inertial, elastic and aerodynamic forces. Studies on transonic flutter are important in the design of aircrafts which operate in the transonic regime. Moreover, as compressibility effects are very important in transonic flow, a compressible aerodynamic theory must be used to model the unsteady aerodynamic behavior.

The various methods that are used for flutter analysis of a two dimensional airfoil differ in the prediction of aerodynamic loads. The lift and moment predictions on an airfoil undergoing harmonic motion have been obtained by Theodorsen [1]. Several CFD methods which are used to determine the transonic flowfield around two dimensional airfoils are listed by Ballhaus and Bridgeman [2]. Ballhaus and Goorjian [3] performed time-marching transonic flutter predictions using the transonic aerodynamic code LTRAN2. Yang *et al.* [4] performed flutter analysis of the NACA 64A006 airfoil with pitching and plunging degrees of freedom using aerodynamic coefficients obtained from the transonic codes UTRANS2 and LTRAN2. Guruswamy and Yang [5] used the LTRAN2 code for studies on aeroelastic time response analysis of airfoils. The aerodynamic force and moment response of an airfoil can be represented by indicial functions. Indicial response for an incompressible flow was obtained theoretically by Wagner [6]. Jones [7] used a two-pole exponential approximation to the Wagner function. Venkatesan and Friedmann [8] have given a three-pole indicial response function that can express the Theodorsen's function over the entire reduced frequency range.

Flutter analysis of wings are also done using different representations of the aerodynamic loads. Kapania, Bergen and Barthelemy [9] have used the Yates modified strip analysis [10] for representation of the unsteady aerodynamic loads in obtaining the flutter

response of a laminated wing. A recent review of various studies in unsteady transonic flow calculations was given by Tjatra [11]. Advanced codes such as XTRAN3S [12] and CAP-TSD [13], which use the transonic small disturbance equation are currently being used for aeroelastic analysis.

Leishman and Nguyen [14] have represented the aerodynamic indicial response functions for compressible flow by upto three-pole approximations, the response consisting of two parts, one due to non-circulatory loading and the other due to circulatory loading. This has advantages over the CFD-based methods in the sense that the CFD methods are in general computationally very expensive.

In recent years, considerable efforts are being made to integrate the aerodynamic, structural and control aspects of the design of an aircraft. Livne [15] notes that for integrated multidisciplinary wing synthesis, where design for aeroservoelastic stability is an objective, it is required to represent the aeroelastic equations of motion in Linear Time Invariant (LTI) state-space form. The unsteady aerodynamic loads on the wing can be represented in a state-space form, thereby adding only a small number of states to the mathematical model of the aeroservoelastic system.

Sensitivity analysis is becoming an important design tool in engineering design applications. It was first recognized as a useful tool for assessing the effects of changing parameters in mathematical models of control systems. The gradient based mathematical programming method used in optimal control and structural optimization furthered the development of sensitivity derivatives, because sensitivity derivatives are used in search directions to find optimum solution [16]. Sensitivity analysis has also become a versatile design tool, rather than just an instrument of optimization programs [17]. Sobieski [18] discusses in detail about the System Design Derivatives which help in understanding the

effect a particular design variable would have on the desired performance of the system, if it were perturbed by a small percentage from its original value.

The sensitivity derivatives of a system can be found using either analytical or finite difference methods. Analytical sensitivity analysis has found increased interest in engineering design as it eliminates uncertainity in the choice of step size needed in the finite difference method. The step size if too large leads to truncation errors and if too small leads to ill-conditioning.

Adelman and Haftka [17] have shown that structural sensitivity analysis has been available for over two decades. Structural sensitivity analysis has been sufficient in the past because sizing variables such as plate thickness and cross-sectional areas affect the mass and stiffness properties of the airframe, but, not its basic geometry. Therefore, aerodynamic sensitivity analysis capability has been limited in development until recently. For example, Rudisill and Bhatia [19] developed expressions for the analytical derivatives of the eigenvalues, reduced frequency and flutter speed with respect to structural parameters for use in minimizing the total mass.

Pedersen and Seyranian [20], examined the change in flutter load as a function of change in stiffness, mass, boundary conditions or load distribution. They showed how sensitivity analysis can be performed without any new eigenvalue analysis. The solution to the main and an adjoint problem provide all the necessary information for evaluating sensitivities. Their paper mainly focused on column and beam critical load distributions.

Hawk and Bristow [21] developed aerodynamic sensitivity analysis capabilities in subcritical compressible flow. They first analyzed a baseline configuration, and then calculated a matrix containing partial derivatives of the potential at each control point with respect

to each known geometric parameter by applying a first order expansion to the baseline configuration. The matrix of partial derivatives is used in each iteration cycle to analyze the perturbed geometry. However, this analysis only handles chordwise perturbation distributions, such as changes in camber, thickness and twist. A new approach, which is still under development, has been presented by Yates [22] that considers general geometric variations, including planform, and subsonic, sonic and supersonic unsteady, nonplanar lifting-surface theory.

Recently, Livne *et al* [23] applied an equivalent plate structural modeling, which includes transverse shear, to an HSCT wing. Simple polynomials were used for Ritz functions and depth and thickness distributions. The derivatives of the stiffness and mass matrices were obtained analytically with respect to the shape variables of the wing. Livne [24] observed that as higher order polynomials are used for better modeling of the structure, the more sensitive is the finite difference derivative to the step-size used and in some cases, it is impossible to obtain any valuable information by finite differences.

Barthelemy and Bergen [25] explored the analytical shape sensitivity derivatives of the wing's aeroelastic characteristics, such as section lift, angle of attack, rolling moment, induced drag and divergence dynamic pressure, for subsonic subcritical flow, with respect to geometric parameters. Results showed the characteristics nonlinearity to be small enough to be well approximated by sensitivity based linear approximations. These approximations are valid within a range that is useful to designers in the initial design phase.

Kapania [26] has obtained sensitivity derivatives of the flutter speed of a two dimensional airfoil in incompressible flow with respect to the mass and stiffness parameters. Kapania, Bergen and Barthelemy [9] have obtained the shape sensitivity derivatives of the

flutter response of a laminated wing in incompressible flow. In this work, Yates' modified strip analysis [10] was used for the aerodynamic model in conjunction with Giles' equivalent plate analysis [27,28] for the structural model.

Sensitivity derivatives are of great importance in integrated multidisciplinary design optimization of aircrafts. Karpel [29] used a gradient-based constrained optimization on a composite active-flexible wing to achieve aircraft performance requirements and sufficient flutter and control stability margins with a minimum weight penalty and without violating the design constraints. The sensitivity derivatives of the flutter dynamic pressure, control stability margins and control effectiveness with respect to structural and control design variables were obtained analytically.

Hajela *et al* [30] applied Sobieski's Global Sensitivity Equations (GSE) in an aircraft synthesis problem where the constraints involved the coupled disciplines of structures, aerodynamics and flight mechanics. The coupled system was represented by smaller subsystems and the total behavior sensitivities were determined by applying the GSE method.

Barthelemy *et al* [31] discuss a multidisciplinary design optimization method applied to a supersonic transport wing. Aerodynamic and structural disciplines are integrated for a minimum weight design under static aeroelastic constraints. He points out that as the number of dependent variables in each discipline becomes large, the calculation of the finite difference derivatives contributes substantially to the total optimization cost.

In this paper, the flutter speed of a two degree of freedom airfoil with plunging and pitching degrees of freedom in transonic flow is determined. The aerodynamic force and moment response are represented by indicial response functions as given by Leishman and Crouse [32]. The resulting aerodynamic state equations are coupled with the structural

equations and the stability of the aeroelastic model so obtained is determined using an eigenanalysis. Flutter calculations are also performed in the time-domain using the Wilson-θ method and the results compared with the eigenanalysis results. The flutter speed of the airfoil is estimated and the sensitivity derivatives of the flutter speed with respect to various parameters, namely, mass ratio, static unbalance, radius of gyration, bending frequency and torsional frequency are calculated by both analytical and finite difference methods. The aerodynamic state-space model [14] is then modified to represent the unsteady aerodynamic forces on a wing. The wing structure is modelled as a wing box and Chebyshev polynomials are chosen for the displacement function. The aeroelastic equations for the wing are solved as an eigenvalue problem to determine the stability. The derivatives of the flutter speed are calculated with respect to the shape parameters, namely (i) aspect ratio, (ii) area, (iii) taper ratio, and (iv) sweep, by analytical and finite difference methods. To the best of our knowledge, this is a first study on the sensitivity analysis of the flutter response in transonic flow.

2. AERODYNAMIC MODEL

In recent years, considerable efforts are being made to integrate the aerodynamic, structural and control aspects of the design of an aircraft. Since the control and the structural dynamic behaviors can easily be expressed in terms of the state-space form (i.e., in terms of a set of first order ordinary differential equations in time), it is desirable that the unsteady aerodynamic airloads be also expressed in the same form. In recent years, considerable efforts have been made in that direction.

The state-space approach has the advantage that any system of differential equations can be represented by a set of first order ordinary differential equations of the form

$$\dot{\mathbf{x}} = \mathbf{A}\mathbf{x} + \mathbf{B}\mathbf{u}$$

with the output equations given by

$$\mathbf{y} = \mathbf{C}\mathbf{x} + \mathbf{D}\mathbf{u} \tag{1}$$

where $\mathbf{x}$ are the aerodynamic state variables, $\mathbf{u}$ are the system inputs and $\mathbf{y}$ are the system outputs. If the unsteady aerodynamic behavior can be represented by state equations, then they can be easily coupled to the structural equations of motion and the resulting system can be examined for aeroelastic stability.

The aerodynamic force and moment response of an airfoil can be represented by indicial functions. For example, Jones [7] used a two-pole exponential approximation to the Wagner function [6] given by

$$\phi(S) = 1 - 0.165exp(-0.0455S) - 0.335exp(-0.3S) \tag{2}$$

where $S = 2Vt/c$, V is the freestream velocity, t is the time and c is the chord. The state equations describing the unsteady aerodynamic response can then be obtained by the

application of Laplace transforms to these indicial functions. The resulting state equations are

$$\begin{Bmatrix} \dot{x_1} \\ \dot{x_2} \end{Bmatrix} = \begin{bmatrix} 0 & 1 \\ -0.01375(\frac{2V}{c})^2 & -0.3455(\frac{2V}{c}) \end{bmatrix} \begin{Bmatrix} x_1 \\ x_2 \end{Bmatrix} + \begin{Bmatrix} 0 \\ 1 \end{Bmatrix} \alpha_{3/4}(t) \tag{3}$$

with the output equation given by

$$C_N(t) = 2\pi[0.006825(\frac{2V}{c})^2 \quad 0.10805(\frac{2V}{c})] \begin{Bmatrix} x_1 \\ x_2 \end{Bmatrix} + 0.5\alpha_{3/4}(t) \tag{4}$$

where C_N is the normal force coefficient and α is the angle of attack.

In this paper, the state-space representation given by Leishman and Nguyen [14] has been used to represent the compressible unsteady aerodynamics. The indicial normal force and quarter chord pitching moment responses to a step change in angle of attack α and a step change in pitch rate q can be written as [14]

$$\begin{aligned}
\frac{C_N(S)}{\alpha} &= \frac{4}{M}\phi_\alpha^I(S,M) + C_{N_\alpha}(M)\phi_\alpha^C(S,M) \\
\frac{C_M(S)}{\alpha} &= -\frac{1}{M}\phi_{\alpha M}^I(S,M) + C_{N_\alpha}(M)\phi_\alpha^C(S,M)(0.25 - x_{ac}(M)) \\
\frac{C_N(S)}{q} &= \frac{1}{M}\phi_q^I(S,M) + \frac{C_{N_\alpha}(M)}{2}\phi_q^C(S,M) \\
\frac{C_M(S)}{q} &= -\frac{7}{12M}\phi_{qM}^I(S,M) - \frac{C_{N_\alpha}(M)}{16}\phi_{qM}^C(S,M)
\end{aligned} \tag{5}$$

where $\phi_\alpha^C, \phi_\alpha^I, \phi_{\alpha M}^I, \phi_q^C, \phi_{qM}^C, \phi_{qM}^I$ are exponential functions of S and M. Here, M is the Mach number, $q = \dot{\alpha}c/V$ is the pitch rate, C_N is the normal force coefficient, C_M is the pitching moment coefficient about the quarter chord and C_{N_α} is the normal force curve slope. The superscripts C and I refer to circulatory and non-circulatory components of the indicial response functions. Note that $\frac{2\pi}{\beta}$ (where $\beta = \sqrt{1-M^2}$ is the compressibility factor) in [14] has been replaced by $C_{N_\alpha}(M)$, so that experimental values of C_{N_α} obtained as functions of Mach number can be used.

The aerodynamic state equations have been shown by Leishman and Nguyen [14] to be given by

$$\dot{\mathbf{x}} = \mathbf{A}\mathbf{x} + \mathbf{B}\begin{Bmatrix} \alpha \\ q \end{Bmatrix} \tag{6}$$

where

$$\mathbf{A} = diag[\, a_{11}\ a_{22}\ a_{33}\ a_{44}\ a_{55}\ a_{66}\ a_{77}\ a_{88}\,]$$

$$\mathbf{B} = \begin{bmatrix} 1 & 1 & 1 & 0 & 1 & 1 & 0 & 0 \\ 0.5 & 0.5 & 0 & 1 & 0 & 0 & 1 & 1 \end{bmatrix}^T$$

The output equations are given by

$$\begin{Bmatrix} C_N \\ C_M \end{Bmatrix} = \mathbf{C}\mathbf{x} + \mathbf{D}\begin{Bmatrix} \alpha \\ q \end{Bmatrix} \tag{7}$$

where

$$\mathbf{C} = \begin{bmatrix} c_{11} & c_{12} & c_{13} & c_{14} & 0 & 0 & 0 & 0 \\ c_{21} & c_{22} & 0 & 0 & c_{25} & c_{26} & c_{27} & c_{28} \end{bmatrix}$$

$$\mathbf{D} = \begin{bmatrix} 4/M & 1/M \\ -1/M & -7/12M \end{bmatrix}$$

The nonzero terms of the a_{ij}'s and c_{ij}'s are given in the Appendix.

3. FLUTTER ANALYSIS OF THE AIRFOIL

AEROELASTIC MODEL

The aerodynamic equations in state-space form can be coupled to the structural equations of motion of an airfoil section with bending and torsional degrees of freedom. The equations of motion for the airfoil section shown in Fig.1 can be written as

$$\begin{aligned} m\ddot{h} + S_\theta\ddot{\theta} + g_h\dot{h} + m\omega_h^2 h &= Q_h \\ S_\theta\ddot{h} + I_\theta\ddot{\theta} + g_\theta\dot{\theta} + I_\theta\omega_\theta^2\theta &= Q_\theta \end{aligned} \tag{8}$$

where $m = \pi\mu\rho(c/2)^2$ is the mass per unit length, μ is the mass ratio, ρ is the air density, $I_\theta = m(c/2)^2 r_\theta^2$ is the polar moment of inertia about the quarter chord per unit length, r_θ is the radius of gyration about elastic axis, $S_\theta = m(c/2)x_\theta$ is the static mass moment, x_θ is the nondimensional distance in semichords from elastic axis to center of mass, h is the plunge displacement (positive downward), θ is the pitch angle, ω_h and ω_θ are the bending and torsion frequency respectively, g_h and g_θ are the structural damping coefficients in plunging and pitching respectively and Q_h and Q_θ are generalized aerodynamic forces in plunging and pitching respectively.

By defining the states

$$z_1 = h,\ z_2 = \theta,\ z_3 = \dot{h},\ z_4 = \dot{\theta}, \tag{9}$$

the above equations can be written as

$$\begin{bmatrix} \mathbf{I} & 0 \\ 0 & \mathbf{M} \end{bmatrix} \dot{\mathbf{z}} = \begin{bmatrix} 0 & \mathbf{I} \\ -\mathbf{k} & -\mathbf{g} \end{bmatrix} \mathbf{z} + \begin{Bmatrix} 0 \\ \mathbf{Q} \end{Bmatrix} \tag{10}$$

where

$$\mathbf{M} = \begin{bmatrix} m & S_\theta \\ S_\theta & I_\theta \end{bmatrix} \qquad \mathbf{g} = \begin{bmatrix} g_h & 0 \\ 0 & g_\theta \end{bmatrix}$$

$$\mathbf{k} = \begin{bmatrix} m\omega_h^2 & 0 \\ 0 & I_\theta \omega_\theta^2 \end{bmatrix}$$

$$\mathbf{Q} = \begin{Bmatrix} -L \\ M \end{Bmatrix} = \frac{1}{2}\rho V^2 \begin{bmatrix} -c & 0 \\ 0 & c^2 \end{bmatrix} \begin{Bmatrix} C_N \\ C_M \end{Bmatrix}$$

In order to couple the structural and aerodynamic equations, the input vector can be expressed in terms of the z states as given below

$$\begin{Bmatrix} \alpha \\ q \end{Bmatrix} = \begin{bmatrix} 0 & 1 & 1/V & 0 \\ 0 & 0 & 0 & c/V \end{bmatrix} \begin{Bmatrix} z_1 \\ z_2 \\ z_3 \\ z_4 \end{Bmatrix} \tag{11}$$

The aerodynamic state equations and the output equations then respectively become

$$\begin{aligned} \dot{\mathbf{x}} &= \mathbf{A}\mathbf{x} + [\mathbf{B}_1' \ \mathbf{B}_2']\mathbf{z} \\ \mathbf{Q} &= \mathbf{C}'\mathbf{x} + [\mathbf{D}_1' \ \mathbf{D}_2']\mathbf{z} \end{aligned} \tag{12}$$

where $\mathbf{A}$ is a diagonal 8x8 matrix, $\mathbf{B}_1'$ and $\mathbf{B}_2'$ are 8x2 matrices, $\mathbf{C}'$ is a 2x8 matrix and $\mathbf{D}_1'$ and $\mathbf{D}_2'$ are 2x2 matrices.

The resulting set of first-order differential equations in terms of the $\mathbf{z}$ and $\mathbf{x}$ states are given by

$$\begin{bmatrix} \mathbf{I} & 0 & 0 \\ 0 & \mathbf{M} & 0 \\ 0 & 0 & \mathbf{I} \end{bmatrix} \begin{Bmatrix} \dot{\mathbf{z}} \\ \dot{\mathbf{x}} \end{Bmatrix} = \begin{bmatrix} 0 & \mathbf{I} & 0 \\ \mathbf{D}_1' - \mathbf{k} & \mathbf{D}_2' - \mathbf{g} & \mathbf{C}' \\ \mathbf{B}_1' & \mathbf{B}_2' & \mathbf{A} \end{bmatrix} \begin{Bmatrix} \mathbf{z} \\ \mathbf{x} \end{Bmatrix} \tag{13}$$

which is a 12x12 system of linear equations. The stability of the system could be determined at different free-stream speeds by an eigenanalysis of the above system of equations. The flutter speed is that particular value of the free-stream speed at which the real part of the eigenvalue approaches zero.

The aeroelastic equations (13) could also be integrated with respect to time using a time-integration scheme. The Wilson-θ method [33] was used for this purpose. A set of first order ODEs can be represented as

$$[R]\{u'\} = [S]\{u\} \tag{14}$$

In the Wilson-θ method, it is assumed that the variation of acceleration from time t to $t + \theta\Delta t$, where $\theta \geq 1.0$, is linear. At time $(t + \theta\Delta t)$, then

$$\{u_{t+\theta\Delta t}\} = \{u_t\} + \frac{\theta\Delta t}{2}\{u'_{t+\theta\Delta t} + u't\} \tag{15}$$

Then equation (14) becomes

$$\left[[R] - [S]\frac{\theta\Delta t}{2}\right]\{u'_{t+\theta\Delta t}\} = [S]\{u_t + \frac{\theta\Delta t}{2}u'_t\} \tag{16}$$

Using the starting values of $\{u_t\}$ and $\{u'_t\}$ at time t, $\{u'_{t+\theta\Delta t}\}$ is computed from equation (16). The vector $\{u_{t+\theta\Delta t}\}$ is then calculated from equation (15). The new values of $\{u_{t+\theta\Delta t}\}$ and $\{u'_{t+\theta\Delta t}\}$ are then used in equation (16) to update the $\{u'_{t+\theta\Delta t}\}$ vector. The step-by-step integration of the equations is done in this manner with respect to time by repeating the above process. The amplitudes of plunge and pitch displacements are then monitored as time progresses.

4. FLUTTER ANALYSIS OF THE WING

STRUCTURAL MODEL

The structural formulation is based on a Ritz solution technique using the energy functionals for a laminated plate which includes the bending and stretching of the reference surface. The planform geometry can be represented by any generally tapered skewed configuration. The original rectangular (x, y) coordinate system and the transformed (η, ξ) coordinate system of the wing are shown in Fig.2. The $x - y$ plane is the mid-plane of the wing and the z axis is normal to the wing. For an unswept wing the fiber angle is measured counterclockwise from the positive y axis. As the wing is swept, the fiber angle is also rotated correspondingly.

In the Rayleigh-Ritz formulation, Chebyshev polynomials T_i are used to represent the displacements at any point on the wing[34]. The Chebyshev polynomials are given by

$$\begin{aligned} T_0(\psi) &= 1 \\ T_1(\psi) &= \psi \\ T_i(\psi) &= 2\psi T_{i-1} - T_{i-2} \qquad -1 \leq \psi \leq 1 \end{aligned} \tag{17}$$

The displacements are expressed in terms of the Chebyshev polynomials as shown

$$\begin{aligned} U(\eta,\xi) &= \sum_{i=0}^{I}\sum_{j=0}^{J} R_{ij} T_i(\eta) T_j(\xi) \\ V(\eta,\xi) &= \sum_{k=0}^{K}\sum_{l=0}^{L} S_{kl} T_k(\eta) T_l(\xi) \\ W(\eta,\xi) &= \sum_{m=0}^{M}\sum_{n=0}^{N} P_{mn} T_m(\eta) T_n(\xi) \qquad -1 \leq \eta, \xi \leq 1 \end{aligned} \tag{18}$$

It has been shown by Singhvi and Kapania [34] that for free vibrations of the laminated composite wing (*i.e.*, in the absence of aerodynamic forces) the equations of motion can

be derived using classical plate theory in the form

$$[M]\{\ddot{q}\} + [\bar{K}]\{q\} = 0 \tag{19}$$

where $[\bar{K}]$ and [M] are the stiffness and mass matrices. The eigenvector $\{q\}$ is defined as

$$q = (R_{00}, R_{01}, ...R_{ij}; S_{00}, S_{01}, ...S_{kl}; P_{00}, P_{01}, ...P_{mn})^T \tag{20}$$

Linear and rotational springs of large magnitude are placed at the wing root to satisfy the clamped boundary conditions. The stiffness matrix for the plate alone (*i.e.*, excluding the springs) is

$$[\bar{K}] = \int_{-1}^{1}\int_{-1}^{1}[B]^T[T]^T\begin{bmatrix} A & B \\ B & D \end{bmatrix}[T][B]|J|d\eta d\xi \tag{21}$$

where $[B]$ is the matrix whose elements consist of the partial derivatives of the Chebyshev polynomials with respect to the natural coordinates η and ξ and is defined by

$$\begin{pmatrix} \epsilon' \\ \kappa' \end{pmatrix} = [B]\{q\} \tag{22}$$

where

$$\begin{pmatrix} \epsilon' \\ \kappa' \end{pmatrix}^T = (u_\eta \;\; u_\xi \;\; v_\eta \;\; v_\xi \;\; w_\eta \;\; w_{\eta\eta} \;\; w_{\xi\xi} \;\; w_{\eta\xi})$$

The $[T]$ in equation(21) is the transformation matrix that relates the strain and curvature vector in the (x, y) coordinate system to the strain and curvature vector in the (η, ξ) coordinate system and J is the Jacobian of the transformation. The strain transformation is given by

$$\begin{pmatrix} \epsilon \\ \kappa \end{pmatrix} = [T]\begin{pmatrix} \epsilon' \\ \kappa' \end{pmatrix} \tag{23}$$

where

$$\begin{pmatrix} \epsilon \\ \kappa \end{pmatrix}^T = (u_x \;\; v_y \;\; u_y + v_x \;\; w_{xx} \;\; w_{yy} \;\; 2w_{xy})$$

The details of the $[T]$ and $[B]$ matrices and J are given in [35]. A typical element of the mass matrix $[M]$ is given by

$$M_{ij} = \int_{-1}^{1} \int_{-1}^{1} T_k(\eta) T_l(\xi) T_o(\eta) T_p(\xi) |J| d\eta d\xi \tag{24}$$

The coefficients R_{ij} and S_{kl} in $\{q\}$ corresponding to the inplane displacements in equation(19) are condensed out using static condensation to the form

$$[M]\{\ddot{P_{mn}}\} + [K]\{P_{mn}\} = 0 \tag{25}$$

where $[M]$ is the mass matrix and $[K]$ is the stiffness matrix of order $(m+1)$x$(n+1)$ with generalized coefficients $\{P_{mn}\}$. In the present work, a value of 5 is chosen for both m and n.

AEROELASTIC MODEL

The aerodynamic state space model which was used for the aeroelastic analysis of a typical section is extended to represent the unsteady aerodynamic forces acting on a wing in transonic flow. The lift and moment forces on a typical section acting at the quarter chord are given by equation(10) as

$$L = \frac{1}{2}\rho V^2 c C_N$$

$$M = \frac{1}{2}\rho V^2 c^2 C_M$$

When extending this compressible aerodynamic theory to a finite span wing, the lift forces are assumed to be distributed along the quarter chord line (reference line) and the moments act about the reference line. Since the lift and moment forces are non-conservative forces, using the principle of virtual work, we get

$$\delta W_{nc} = \int_0^l -L\delta h d\bar{y} + \int_0^l M\delta\theta d\bar{y} \tag{26}$$

where l is the length of the quarter chord line, δh and $\delta\theta$ are virtual displacements and $\bar{y}$ is the coordinate along the reference line.

The displacement at any location $\bar{y}$ is given by

$$h(\bar{y}) = w(\eta, \xi) \tag{27}$$

where η and ξ are the natural coordinates corresponding to the (x, y) coordinates of the point at distance $\bar{y}$ from the origin.

The rotation about the reference line is given by

$$\theta(\bar{y}) = w_{,x}\, cos\Lambda - w_{,y}\, sin\Lambda \tag{28}$$

For facilitating in numerical integration using Gaussian quadrature, the limits of integration along the reference line are transformed in the range of -1 to 1 by $\bar{y} = l(1+\psi)/2$, where $-1 \leq \psi \leq 1$

Substituting the expressions for the lift and moment on the wing and the wing deflection, we have

$$\begin{aligned}
&\int_0^l L\delta h d\bar{y} \\
&\quad = \frac{l}{2}\int_{-1}^{1} L\delta h d\psi \\
&\quad = \frac{l}{2}(\frac{1}{2}\rho V^2 c)\sum_{i=0}^{m}\sum_{j=0}^{n}\left[\int_{-1}^{1}\left\{[C_{1p}]\{x\} + [D_{1p'}]\begin{bmatrix} H_{ij} & 0 \\ 0 & H_{ij} \end{bmatrix}\begin{Bmatrix} P_{ij} \\ \dot{P}_{ij} \end{Bmatrix}\right\} w_1 d\psi\right]\delta P_{ij}
\end{aligned}$$

and

$$\begin{aligned}
&\int_0^l M\delta\theta d\bar{y} \\
&\quad = \frac{l}{2}\int_{-1}^{1} M\delta\theta d\psi \\
&\quad = \frac{l}{2}(\frac{1}{2}\rho V^2 c^2)\sum_{i=0}^{m}\sum_{j=0}^{n}\left[\int_{-1}^{1}\left\{[C_{2p}]\{x\} + [D_{2p'}]\begin{bmatrix} H_{ij} & 0 \\ 0 & H_{ij} \end{bmatrix}\begin{Bmatrix} P_{ij} \\ \dot{P}_{ij} \end{Bmatrix}\right\} w_2 d\psi\right]\delta P_{ij}
\end{aligned} \tag{29}$$

where m and n represent the order of the Chebyshev polynomial used in the displacement function. The row vectors $[C_{1p}]$ and $[C_{2p}]$ are the elements of the $[C]$ matrix (see section on typical section) where $p = 1, 2, \ldots, 8$. The row vectors $[D_{1p'}]$ and $[D_{2p'}]$ are the elements of the matrix given by

$$[D] = \begin{bmatrix} 4/M & 1/M \\ -1/M & -7/12M \end{bmatrix} \begin{bmatrix} 0 & 1 & 1/V & 0 \\ 0 & 0 & 0 & c/V \end{bmatrix} \tag{30}$$

where $p' = 1, \ldots, 4$.

The variables w_1 and w_2 in equation (29) are given by

$$\begin{aligned} w_1 &= T_i(\eta)T_j(\xi) \\ w_2 &= cos\Lambda(T_{i,\eta}T_j\eta_{,x} + T_iT_{j,\xi}\xi_{,x}) - sin\Lambda(T_{i,\eta}T_j\eta_{,y} + T_iT_{j,\xi}\xi_{,y}) \end{aligned} \tag{31}$$

where Λ is the sweep angle.

$[H_{ij}]$ in equation(29) is a matrix of order 2xN where $N = (m+1)(n+1)$. A typical column of the matrix is given by

$$H_k = \begin{Bmatrix} T_iT_j \\ cos\Lambda(T_{i,\eta}T_j\eta_{,x} + T_iT_{j,\xi}\xi_{,x}) - sin\Lambda(T_{i,\eta}T_j\eta_{,y} + T_iT_{j,\xi}\xi_{,y}) \end{Bmatrix} \tag{32}$$

where $k = 1, 2, \ldots, N$.

The column vector $\{x\}$ in equation(29) is the vector of aerodynamic state variables and $\{P_{ij}\ \dot{P}_{ij}\}^T$ is the vector of generalized displacements.

It should be noted that in the integrations performed along the quarter-chord line in equation(29), a constant value of the section lift-curve slope C_{N_α} is used. But for a finite 3D wing, the wing lift-curve slope depends on the planform of the wing which makes C_{N_α} sensitive to the shape variations of the wing.

Using equations(27),(28) and (29), equation(26) can be written as

$$\delta W_{nc} = \sum_{i=1}^{N} Q_i \delta P_i \quad , \qquad N = (m+1)(n+1) \tag{33}$$

where

$$Q_i = [C']\{x\} + [D_1' \; D_2']\begin{Bmatrix} P_{ij} \\ \dot{P}_{ij} \end{Bmatrix} \tag{34}$$

The aerodynamic state equations(6) for a typical section perpendicular to the quarter chord line were in the form

$$\{\dot{x}\} = [A]\{x\} + [B]\{u\}$$

An integration of these state equations along the quarter chord line to consider the effect of finite span yields

$$\begin{aligned} \{\dot{x}\} &= \frac{1}{2}\int_{-1}^{1} \left[[A]\{x\} + [B]\begin{bmatrix} H_{ij} & 0 \\ 0 & H_{ij} \end{bmatrix}\begin{Bmatrix} P_{ij} \\ \dot{P}_{ij} \end{Bmatrix}\right] d\psi \\ &= [A']\{x\} + [B_1' \; B_2']\begin{Bmatrix} P_{ij} \\ \dot{P}_{ij} \end{Bmatrix} \end{aligned} \tag{35}$$

The equation(25) can be written as a set of first order ODE's in $\{P_{ij}\}$ and $\{\dot{P}_{ij}\}$ which will be represented by $\{p_i\}$ and $\{q_i\}$ respectively. It can be coupled with equations(34) and (35) to generate the aeroelastic equations of the wing in the form

$$\begin{bmatrix} I & 0 & 0 \\ 0 & M & 0 \\ 0 & 0 & I \end{bmatrix}\begin{Bmatrix} \dot{p}_i \\ \dot{q}_1 \\ \dot{x} \end{Bmatrix} = \begin{bmatrix} 0 & I & 0 \\ D_1' - k & D_2' & C' \\ B_1' & B_2' & A' \end{bmatrix}\begin{Bmatrix} p_i \\ q_i \\ x \end{Bmatrix} \tag{36}$$

Since a Chebyshev polynomial of order 5 is chosen for the displacement function in η and ξ, we have 36 generalized coefficients $\{p_i\}$, their 36 time derivatives $\{q_i\}$ and the 8 aerodynamic state variables $\{x\}$. The stability of this system can be determined by solving an 80x80 eigenvalue problem.

5. SENSITIVITY ANALYSIS

The aeroelastic equations obtained as a set of first order ODEs is of the form

$$[P]\dot{\mathbf{w}} = [Q]\mathbf{w} \tag{37}$$

which could be written as

$$\dot{\mathbf{w}} = [E]\mathbf{w} \tag{38}$$

where $[E] = [P]^{-1}[Q]$

The derivative of the ith eigenvalue with respect to the flutter speed is given by

$$\frac{\partial \lambda^i}{\partial V_f} = \frac{\{e_l^i\}^T \frac{\partial [E]}{\partial V_f} \{e_r^i\}}{\{e_l^i\}^T \{e_r^i\}} \tag{39}$$

where $\{e_l^i\}$ and $\{e_r^i\}$ are the ith left and right eigenvectors respectively. $\frac{\partial [E]}{\partial V_f}$ is calculated by recomputing the $[E]$ matrix at a slightly higher speed than V_f and using the forward difference technique.

Similarly, the derivative of the ith eigenvalue with respect to any parameter p is given by

$$\frac{\partial \lambda^i}{\partial p} = \frac{\{e_l^i\}^T \frac{\partial [E]}{\partial p} \{e_r^i\}}{\{e_l^i\}^T \{e_r^i\}} \tag{40}$$

$\frac{\partial [E]}{\partial p}$ can be conveniently written as

$$\frac{\partial [E]}{\partial p} = \frac{\partial [P]^{-1}}{\partial p}[Q] + [P]^{-1}\frac{\partial [Q]}{\partial p} \tag{41}$$

and can be computed analytically, where

$$\frac{\partial [P]^{-1}}{\partial p} = -[P]^{-1}\frac{\partial [P]}{\partial p}[P]^{-1}. \tag{42}$$

The analytical derivative of the flutter speed with respect to parameter p is then given by

$$\frac{dV_f}{dp} = -\frac{Real\left(\frac{\partial \lambda^i}{\partial p}\right)}{Real\left(\frac{\partial \lambda^i}{\partial V_f}\right)} \tag{43}$$

The $[E]$ matrix is composed of mass, stiffness and aerodynamic matrices. Obtaining the analytical derivatives of the mass, stiffness and aerodynamic terms with respect to any parameter p is straightforward for the typical section. In the case of the finite wing, the expressions for the analytical derivatives of the $[\bar{K}]$ and $[M]$ matrices (equations(21) and (24)) are given in [35]. Since the reduced stiffness matrix $[K]$ is obtained from $[\bar{K}]$ by static condensation the analytical derivative $\frac{\partial [K]}{\partial p}$ is obtained by a succession of differentiations using the chain rule. The derivatives of the aerodynamic terms are obtained by taking the analytical derivatives of those terms that are explicit functions of the shape parameters, given in the Appendix.

6. EVALUATION ANALYSIS

The flutter characteristics of the airfoil are found by calculating the complex eigen values $\lambda_k = \sigma_k + i\omega_k$ at various values of free stream velocity. Flutter occurs at the lowest speed for which any σ_k becomes positive.

The flutter speed was determined for the following case, the results for which have been presented by Leishman and Crouse [32]. The parameters used are $\mu = 100$, $x_\theta = 0.25$, $r_\theta = 0.5$, $\omega_h = 10\ rad/s.$, $\omega_\theta = 50\ rad/s.$, $a_h = -0.5, b = 5\ in.$, $C_{N_\alpha} = 14.65$, $x_{ac} = 0.286$, $M = 0.85$. Flutter was found to occur at 92.34 ft/s., i.e., a non-dimensional speed of $V/b\omega_\theta$=4.43 which agrees well with the value of $V/b\omega_\theta$=4.4 reported in [32].

The damping ratio for each of the aeroelastic modes is given by

$$\zeta_k = -\frac{\sigma_k}{\sqrt{\sigma_k^2 + \omega_k^2}} \tag{44}$$

A plot of the variation of the damping ratio ζ with non-dimensional speed $V/b\omega_\theta$ is given in Fig.3. Fig.4 shows the variation of flutter speed predicted by this theory for different values of ω_h/ω_θ.

The flutter analysis was also carried out in the time-domain for comparison with the results obtained from the eigenanalysis. A time-integration of the first order ODEs representing the aeroelastic system was done using the Wilson-θ method. The plunge and pitch amplitudes of motion are plotted with respect to time in Figs. 5 and 6 respectively, at three different non-dimensional speeds, including the flutter speed. It can be seen that at speeds below the flutter speed, the oscillations that are set in due to any initial disturbance given to the airfoil die out as time progresses, whereas, at speeds above the flutter speed, the displacement amplitudes increase with time, leading to instability. At the flutter speed,

the oscillations are able to maintain a constant amplitude, denoting a neutrally stable condition.

The sensitivity of flutter speed with various parameters namely μ, x_θ, r_θ, ω_h and ω_θ was calculated by both analytical and finite difference methods. In the analytical method, the derivatives of the [E] matrix (see section on Sensitivity Analysis) with respect to the above mentioned parameters were calculated analytically. The finite difference derivatives were calculated for step sizes of 1%, 0.1% and 0.01%. The parameters were perturbed one at a time using these step sizes and the flutter speed recomputed. A forward difference scheme was then applied to compute the derivatives. It can be seen from the results shown in Table 1 that the forward difference derivatives obtained using a step size of 0.01% have good agreement with the analytical values.

Figs. 7 – 11 show the variation of flutter speed obtained by eigenanalysis with respect to various parameters. In each case, the sensitivity derivative computed at a particular value of the parameter is also shown.

Having gained confidence in the accurate prediction of the sensitivity derivatives, the sensitivity derivatives were computed both analytically and by finite difference method for a range of transonic Mach numbers. The $C_{N_\alpha}(M)$ and $x_{ac}(M)$ for these calculations were obtained from [4]. The results are tabulated in Table 2. There is good agreement between the analytic derivatives and the finite difference derivatives obtained using a step size of 0.01%.

Before performing the sensitivity calculations of the flutter speed of the wing with respect to shape parameters, comparison of natural frequencies and predicted flutter speeds was made with results from other sources. The first three natural frequencies of an unswept

wing and its flutter speed in subsonic flow were compared with results reported by Landsberger and Dugundji [36] for different laminate sequences in Table 3 and Table 4. The material used for the wing is Hercules Graphite Epoxy (AS1/3501-6) with properties: $E_1 = 98$ x 10^9 Pa, $E_2 = 7.9$ x 10^9 Pa, $\nu_{12} = 0.28$, $G_{12} = 5.6$ x 10^9 Pa and $\rho = 1520$ kg/m^3. The thickness of each ply is 0.134 x 10^{-3} m. The flutter data used for comparison [36] are the experimental results from the wind tunnel tests performed in the MIT Acoustic wind tunnel. The results agree fairly well.

An experimental investigation of the flutter characteristics of the wing in transonic flow was performed in the Langley transonic dynamics tunnel, the results of which have been reported by Yates [37]. The 2.5 foot weakened 3 model is used for comparison with our results. The material properties of the laminated mahogany wing are: $E_1 =$ 0.47072 x 10^6 psi, $E_2 =$ 0.01883 x 10^6 psi, $\nu_{12} = 0.28$, $G_{12} =$ 0.05975 x 10^7 psi and $\rho =$ 0.60267 $slug/ft^3$. The wing dimensions are: $Area = 3.782$ ft^2, $Aspect\ ratio =$ 1.6525, $Taper\ ratio = 0.6576$, $Sweep(1/4\ chord) = 45^o$ and $thickness = 0.056$ ft. The natural frequencies for the wing obtained from the present analysis is compared with the measured natural frequencies from [37] in Table 5. A good agreement is obtained. The flutter speed obtained from this analysis is compared with the non-dimensional flutter data measured in air for the WEAK3 model [37] at different Mach numbers in Table 6. The non-dimensionalizing parameter used is $b_s\omega_\alpha\sqrt{\mu}$ where μ is the mass ratio, b_s is the root semichord, and ω_α is the angular frequency of the first torsion mode. For this model, b_s and ω_α are 0.9165 ft and 230.9 rad/s respectively. It should be noted that the 2.5 foot WEAK3 model has a low aspect ratio of 1.6525. In our aerodynamic model, we have assumed the lift forces to be acting along the quarter chord line and the moments about the quarter chord line, which is a good assumption for high aspect ratio wings. In reality

however, the aerodynamic forces and moments are distributed over the surface of the wing. Yet, the flutter results obtained are encouraging.

Having achieved good prediction of flutter speeds, sensitivity analysis of the flutter speed of the wing with respect to shape parameters is carried out. The wing box is shown in Fig.12. The wing skins are made of 0^o laminated Graphite/Epoxy ($T300/N5208$) with the following material properties: $E_1 = 181$ x 10^9 Pa, $E_2 = 10.3$ x 10^9 Pa, $\nu_{12} = 0.28$, $G_{12} = 7.17$ x 10^9 Pa and $\rho = 1600$ kg/m^3. The critical airspeed of the wing is shown in Fig.13 as a function of the quarter-chord sweep angle. As seen from the graph, divergence (zero frequency flutter) instability is critical upto a sweep angle of about 16^o and for higher sweep angles, the flutter mode is the unstable mode. Tables 7 and 8 give the shape sensitivity derivatives of the divergence speeds and flutter speeds of a wing at Mach 0.9. The analytical shape derivatives agree well with the finite difference derivatives obtained with a stepsize of 0.01%.

The critical speeds of the wing obtained by perturbing one shape parameter at a time from the baseline configuration are shown in Fig.14–21. The prediction of critical speed by analytical sensitivity calculations is also superposed. The sensitivity derivative obtained forms a tangent to the critical speed curve at the value of the shape parameter at which it is computed.

In order to observe the aeroelastic phenomena in real time, one of the coefficients of the displacement function was perturbed and the system of equations(36) was integrated with respect to time using the Wilson-θ method. The wing tip displacement is plotted as a function of time at different speeds in Fig.22-28. The tip displacement of the unswept wing at the divergence speed is shown in Fig.22. It can be seen that the displacement approaches a constant amplitude at this speed. Above this speed, the displacement increases with time

as shown in Fig.23. For the 15^o swept wing, the displacement slowly approaches a constant value at the divergence speed as shown in Fig.24. The oscillatory nature is due to the fact that the flutter and divergence speeds are close enough. Fig.25 shows the flutter condition for the 15^o swept wing. Since the wing has already diverged at a lower speed, we see the constant amplitude oscillations about a diverging mean position. Fig.26, 27 and 28 show the tip displacement of the 30^o swept wing below the flutter speed, at the flutter speed and above the flutter speed, respectively.

The lift-curve slope of a finite wing depends on the planform of the wing and hence is sensitive to shape variations of the wing. For a finite wing in compressible flow, the wing lift-curve slope as given by Hauptman and Miloh [38] can be written as

$$C_{N_\alpha} = \frac{4}{\left[k + \frac{E^2(h)}{k+(arcsin\ h)/h}\right]} \frac{1}{\sqrt{1 - M^2 cos^2 \Lambda}} \tag{45}$$

where $k = 4/\pi AR$ and $h = \sqrt{(1-k^2)}$ and AR is the aspect ratio of the wing. $E(h)$ is the complete elliptic integral of the second kind and is given by

$$E(h) = \int_0^{\pi/2} (1 - h^2 sin^2\phi)^{1/2}\ d\phi \tag{46}$$

Using the above expression for the wing lift-curve slope in equation(29), the flutter calculations were carried out. The critical airspeed of the wing is shown in Fig.29 by varying the sweep angle of the wing. The sensitivity of the flutter speed of the wing with respect to shape parameters and the flutter speeds obtained from reanalysis by perturbing one shape parameter at a time are shown in Fig.30-33. The sensitivity derivative forms a tangent to the flutter speed curve at the baseline configuration and gives a linear approximation to the flutter speeds within a certain range, about the baseline value.

7. CONCLUDING REMARKS

The dynamic aeroelastic behavior of a two degree of freedom airfoil, with plunging and pitching degrees of freedom, was examined using a state-space approach in the transonic flow regime. The indicial response functions presented by Leishman and Nguyen [14] were used to represent the unsteady aerodynamic behavior. The flutter speed of the airfoil was determined using an eigen analysis of a system of 12 first order ordinary differential equations. The results obtained from the eigenanalysis was compared wth the results obtained by performing a time-integration of the aeroelastic equations. The sensitivities of the flutter speed with respect to the mass and stiffness parameters were computed by both analytical and finite difference methods and the results obtained are in excellent agreement with each other.

The compressible unsteady aerodynamic theory using indicial response functions was successfully modified to represent the aerodynamic forces and moments on a finite span wing. Using this aerodynamic state-space model and the structural formulation based on Ritz technique, flutter analysis of wings were carried out in transonic flow. The use of Chebyshev polynomials for Ritz functions gives the added benefit of closed form analytical expressions for the derivatives of stiffness and mass matrices with respect to the shape design parameters of the wing. This avoids the uncertainities and the computational expense associated with finite difference derivative calculations. The shape sensitivity derivatives of the critical speed of the wing were computed by analytical and finite difference methods and they are in excellent agreement with each other. These shape derivatives of the flutter response of a wing in transonic flow would be very useful to a designer in the initial design phase, thus avoiding the necessity of a reanalysis for small changes in the design parameters.

REFERENCES

(1.) Theodorsen, T., "General Theory of Aerodynamic Instability and the Mechanism of Flutter," NACA Rept. 496, 1935.

(2.) Ballhaus, W.F., and Bridgeman, J.O., "Numerical Solution Techniques for Unsteady Transonic Problems," AGARD Rept. 679, June 1980, pp. 16-1–16-24.

(3.) Ballhaus, W.F., and Goorjian, P.M., "Computation of Unsteady Transonic Flows by the Indicial Method," *AIAA Journal*, Vol. 16, No. 2, 1978, pp. 117-124.

(4.) Yang, T.Y., Guruswamy, P., Stritz, A.G., and Olsen, J.J., "Flutter Analysis of a NACA 64A006 Airfoil in Small Disturbance Transonic Flow," *Journal of Aircraft*, Vol. 17, No. 4, 1980, pp. 225-232.

(5.) Guruswamy, P., and Yang, T.Y., "Aeroelastic Time Response Analysis of Thin Airfoils by Transonic Code LTRAN2," *Journal for Computers and Fluids*, Vol. 9, No. 4, Dec. 1981, pp. 409-425.

(6.) Wagner, H., "Uber die Entstehung des Dynamischen Auftriesbes von Tragflugeln, "*Zeitschrift für Angewandte Mathematik und Mechanic,* Vol. 5, No. 1, Feb. 1925.

(7.) Jones, R.T., "The Unsteady Lift of a Wing of Finite Aspect Ratio," NACA Rept. 681, 1940.

(8.) Venkatesan, C., and Friedmann, P.P., "New Approach to Finite State Modelling of Unsteady Aerodynamics," *AIAA Journal*, Vol. 24, Dec. 1986, pp. 1889-1897.

(9.) Kapania, R.K., Bergen, F.D., and Barthelemy, J.-F.M., "Shape Sensitivity Analysis of Flutter Response of a Laminated Wing," *AIAA Journal*, Vol. 29, No. 4, 1991, pp. 611-612. Also presented at 30th AIAA/ASME/ASCE/AHS/ASC Structures, Structural Dynamics and Materials Conference, Mobile, Alabama, 1989 and NASA-CR-181725.

(10.) Yates, E.C., "Calculation of Flutter Characteristics for Finite-Span Swept or Unswept Wings at Subsonic and Supersonic Speeds by a Modified Strip Analysis," NACA RM L57110, March 1958.

(11.) Tjatra, I.W., "Transonic Aeroelastic Analysis of Systems with Structural Nonlinearities," Ph.D Thesis, Virginia Polytechnic Institute and State University, Blacksburg, VA, April 1991.

(12.) Borland, C.J., and Rizzetta, D.P., "Transonic Unsteady Aerodynamics for Aeroelastic Application, Vol. 1 – Technical Development Summary for XTRAN3S," AFWAL-TR-80-3107, June 1982.

(13.) Batina, J.T., Seidel, D.A., Bland, S.R., and Bennett, R.M., "Unsteady Transonic Flow Calculations for Realistic Aircraft Configurations," AIAA Paper 87-0850, April 1987.

(14.) Leishman, J.G., and Nguyen, K.Q., "State-Space Representation of Unsteady Airfoil Behavior," *AIAA Journal,* Vol. 28, No. 5, May 1990, pp. 836 - 844.

(15.) Livne, E., Schmit, L.A., and Friedmann, P.P., "Towards Integrated Multidisciplinary Synthesis of Actively Controlled Fiber Composite Wings," *Journal of Aircraft*, Vol. 27, No. 12, 1990, pp. 979-992.

(16.) Brayton, R.K., *Sensitivity and Optimization*, Elsevier, New York, 1980.

(17.) Adelman, H.M., and Haftka, R.T., "Sensitivity Analysis of Discrete Structural Systems," *AIAA Journal,* Vol. 24, No. 5, May 1986, pp. 823-831.

(18.) Sobieszczanski-Sobieski, J., "A System Approach to Aircraft Optimization," AGARD Rept. 784, Feb. 1992, pp. 2-1–2-15.

(19.) Rudisill, C.S., and Bhatia, K.G., "Optimization of Complex Structures to Satisfy Flutter Requirements," *AIAA Journal,* Vol. 9, No. 8, August 1971, pp. 1486-1491.

(20.) Pedersen, P., and Seyranian, A.P., "Sensitivity Analysis for Problems of Dynamic Stability," *International Journal of Solids and Structures*, Vol. 19, No. 4, 1983, pp. 315-335.

(21.) Hawk, D.J., and Bristow, D.R., "Development of MCAERO Wing Design Panel Method with Interactive Graphics Module," NASA CR-3775, 1984.

(22.) Yates, E.C., "Aerodynamic Sensitivity from Subsonic, Sonic and Supersonic Unsteady, Nonplanar Lifting Surface Theory," NASA TM-100502, 1987.

(23.) Livne, E., Sels, R.A., and Bhatia, K.G., "Lessons from Application of Equivalent Plate Structural Modeling to an HSCT Wing," Presented at 34th AIAA/ASME/ASCE/AHS/ASC Structures, Structural Dynamics and Materials Conference, La Jolla, California, 1993, AIAA-93-1413.

(24.) Livne, E., "Analytic Sensitivities for Shape Optimization in Equivalent Plate Structural Wing Models," Submitted for publication to *Journal of Aircraft*, 1993.

(25.) Barthelemy, J.-F.M., and Bergen, F.D.,"Shape Sensitivity Analysis of Wing Static Aeroelastic Characteristics," NASA TP-2808, May 1988.

(26.) Kapania, R.K., "Sensitivity Analysis of Dynamic Aeroelastic Responses," AGARD Rept. 784, Feb. 1992, pp. 3-1–3-12.

(27.) Giles, G.L., "Equivalent Plate Analysis of Aircraft Wing Box Structures with General Planform Geometry," *Journal of Aircraft*, Vol. 23, No. 11, Nov. 1986, pp. 859-864.

(28.) Giles, G.L., "Further Generalization of an Equivalent Plate Representation for Aircraft Structural Analysis", NASA TM 89105, Feb. 1987.

(29.) Karpel, M., "Multidisciplinary Optimization of Aeroservoelastic Systems Using Reduced-Size Models," *Journal of Aircraft*, Vol. 29, No. 5, 1992, pp. 939-946.

(30.) Hajela, P., Bloebaum, C.L., and Sobieszczanski-Sobieski, J., "Application of Global Sensitivity Equations in Multidisciplinary Aircraft Synthesis," *Journal of Aircraft*, Vol. 27, No. 12, 1990, pp. 1002-1010.

(31.) Barthelemy, J.-F.M., Coen, P.G., Wrenn, G.A., Riley, M.F., and Dovi, A.R., "Application of Multidisciplinary Optimization Methods to the Design of a Supersonic Transport," AGARD Rept. 784, Feb. 1992, pp. 4-1–4-5.

(32.) Leishman, J.G., and Crouse, G.L., "Transonic Aeroelasticity Analysis Using State-Space Unsteady Aerodynamic Modelling," *Journal of Aircraft*, Vol. 29, No. 1, 1992, pp. 153-160.

(33.) Craig, R.R., *Structural Dynamics – An Introduction to Computer Methods*, John Wiley Publications Inc., 1981.

(34.) Kapania, R.K., and Singhvi, S., "Free Vibration Analysis of Generally Laminated Tapered Skew Plates," *Composites Engineering*, Vol. 2, No. 3, 1992, pp. 197-212.

(35.) Singhvi, S., and Kapania, R.K., "Analysis, Shape Sensitivities and Approximations of Modal Response of Generally Laminated Tapered Skew Plates," CCMS Rept., Virginia Polytechnic Institute and State University, Blacksburg, VA, September 1991.

(36.) Dugundji, J., and Landsberger, B.J., "Experimental Aeroelastic Behavior of Unswept and Forward Swept Cantilever Graphite Epoxy Wings," *Journal of Aircraft*, Vol. 22, No. 8, Aug. 1985, pp. 679-686.

(37.) Yates, E.C., Jr., "AGARD Standard Aeroelastic Configurations for Dynamic Response. Candidate Configuration 1:- Wing 445.6," NASA TM 100492, Aug. 1987.

(38.) Hauptman, A., and Miloh, T., "On the Exact Solution of the Linearized Lifting-Surface Problem of an Elliptic Wing," *Quarterly Journal of Mechanics and Applied Mathematics*, Vo. 39, Feb. 1986, pp. 41-66.

APPENDIX

The a_{ij}'s are given by

$$
\begin{aligned}
a_{11} &= -(\frac{2V}{c})\beta^2 b_1 \\
a_{22} &= -(\frac{2V}{c})\beta^2 b_2 \\
a_{33} &= -\frac{1}{K_\alpha T_I} \\
a_{44} &= -\frac{1}{K_q T_I} \\
a_{55} &= -(b_3 K_{\alpha M} T_I)^{-1} \\
a_{66} &= -(b_4 K_{\alpha M} T_I)^{-1} \\
a_{77} &= -b_5 \beta^2 (\frac{2V}{c}) \\
a_{88} &= -\frac{1}{K_{qM} T_I}
\end{aligned}
\tag{47}
$$

where

$$
\begin{aligned}
K_\alpha(M) &= [(1-M) + \pi\beta M^2(A_1 b_1 + A_2 b_2)]^{-1} \\
K_q(M) &= [(1-M) + 2\pi\beta M^2(A_1 b_1 + A_2 b_2)]^{-1} \\
K_{\alpha M}(M) &= \left[\frac{A_3 b_4 + A_4 b_3}{b_3 b_4 (1-M)}\right] \\
K_{qM}(M) &= \left[\frac{7}{15(1-M) + 3\pi\beta M^2 b_5}\right]
\end{aligned}
\tag{48}
$$

The c_{ij}'s are given by

$$
\begin{aligned}
c_{11} &= C_{N_\alpha}(\frac{2V}{c})\beta^2 A_1 b_1 \\
c_{12} &= C_{N_\alpha}(\frac{2V}{c})\beta^2 A_2 b_2 \\
c_{13} &= \frac{4}{M}(-\frac{1}{K_\alpha T_I}) \\
c_{14} &= \frac{1}{M}(-\frac{1}{K_q T_I}) \\
c_{21} &= C_{N_\alpha}(\frac{2V}{c})\beta^2 A_1 b_1 (0.25 - x_{ac}) \\
c_{22} &= C_{N_\alpha}(\frac{2V}{c})\beta^2 A_2 b_2 (0.25 - x_{ac}) \\
c_{25} &= -\frac{A_3 a_{55}}{M} \\
c_{26} &= -\frac{A_4 a_{66}}{M} \\
c_{27} &= -\frac{C_{N_\alpha}}{16} b_5 \beta^2 (\frac{2V}{c}) \\
c_{28} &= \frac{7}{12M}(\frac{1}{K_{qM} T_I})
\end{aligned}
\tag{49}
$$

The constants are given by $A_1 = 0.3, A_2 = 0.7, A_3 = 1.5, A_4 = -0.5, b_1 = 0.14, b_2 = 0.53, b_3 = 0.25, b_4 = 0.1, b_5 = 0.5$.

Analytical derivatives

Aspect ratio (AR), Area (S), Taper ratio (tr), Sweep (Λ)

The wing coordinates are $x_1,\ x_2,\ x_3\ and\ x_4$.

$$span = \sqrt{AR\ S}$$

$$cr = \frac{2S}{span(1+tr)}$$

$$ct = tr\ cr$$

$$x_1 = 0.75\ cr$$

$$x_2 = span\ tan\Lambda + 0.75\ ct$$

$$x_3 = span\ tan\Lambda - 0.25\ ct$$

$$x_4 = -0.25\ cr$$

$$p = (x_1 + x_2 + x_3 + x_4)$$

$$pp = (x_2 + x_3) - (x_1 + x_4)$$

$$crct = cr + ct$$

$$rt = cr - ct$$

For any point ψ on the quarter chord line ($-1 \leq \psi \leq 1$)

$$y = 0.5\ span\ (1+\psi)$$

$$x = y\ tan\Lambda$$

$$\xi = \frac{2y}{span} - 1$$

$$\eta = \frac{(\xi\ pp - 4x + p)}{(\xi\ rt - crct)}$$

$$c = [cr + (ct - cr)(1+\psi)\ 0.5]\ cos\Lambda$$

Local chord (c)

$$\frac{\partial c}{\partial AR} = -\frac{S^{0.5}[1-(1-tr)(1+\psi)\ 0.5]\ cos\Lambda}{AR^{1.5}(1+tr)}$$
$$\frac{\partial c}{\partial S} = \frac{[1-(1-tr)(1+\psi)\ 0.5]\ cos\Lambda}{\sqrt{AR\ S}(1+tr)}$$
$$\frac{\partial c}{\partial tr} = \frac{cr\ \psi\ cos\Lambda}{(1+tr)}$$
$$\frac{\partial c}{\partial \Lambda} = -c\ tan\Lambda$$

$p = (x_1 + x_2 + x_3 + x_4)$

$$\frac{\partial p}{\partial AR} = \frac{0.5\ S^{0.5}}{AR^{0.5}}\left[2\ tan\Lambda - \frac{1}{AR}\right]$$
$$\frac{\partial p}{\partial S} = \frac{0.5\ p}{S}$$
$$\frac{\partial p}{\partial tr} = 0.0$$
$$\frac{\partial p}{\partial \Lambda} = \frac{2\ span}{cos^2\Lambda}$$

$pp = (x_2 + x_3) - (x_1 + x_4)$

$$\frac{\partial pp}{\partial AR} = 0.5\ S^{0.5}\left[\frac{2\ tan\Lambda}{AR^{0.5}} + \frac{(1-tr)}{(1+tr)\ AR^{1.5}}\right]$$
$$\frac{\partial pp}{\partial S} = \frac{0.5\ pp}{S}$$
$$\frac{\partial pp}{\partial tr} = \frac{cr}{(1+tr)}$$
$$\frac{\partial pp}{\partial \Lambda} = \frac{2\ span}{cos^2\Lambda}$$

$crct = cr + ct$

$$\frac{\partial crct}{\partial AR} = -\frac{S^{0.5}}{AR^{1.5}}$$
$$\frac{\partial crct}{\partial S} = \frac{0.5\ crct}{S}$$
$$\frac{\partial crct}{\partial tr} = 0.0$$
$$\frac{\partial crct}{\partial \Lambda} = 0.0$$

$\underline{rt = cr - ct}$

$$\frac{\partial rt}{\partial AR} = -\frac{S^{0.5}\,(1-tr)}{AR^{1.5}\,(1+tr)}$$
$$\frac{\partial rt}{\partial S} = \frac{0.5\;rt}{S}$$
$$\frac{\partial rt}{\partial tr} = -\frac{2\;cr}{(1+tr)}$$
$$\frac{\partial rt}{\partial \Lambda} = 0.0$$

$\underline{x = y\;tan\Lambda}$

$$\frac{\partial x}{\partial AR} = \frac{S^{0.5}\;tan\Lambda(1+\psi)}{4\;AR^{0.5}}$$
$$\frac{\partial x}{\partial S} = 0.5\;(1+\psi)\;span\;tan\Lambda$$
$$\frac{\partial x}{\partial tr} = 0.0$$
$$\frac{\partial x}{\partial \Lambda} = \frac{0.5\;span\;(1+\psi)}{cos^2\Lambda}$$

$\underline{\eta = (\xi\;pp - 4x + p)/(\xi\;rt - crct)}$

For any parameter v,

$$\frac{\partial \eta}{\partial v} = \frac{(\xi\;rt - crct)(\xi\frac{\partial pp}{\partial v} - 4\;\frac{\partial x}{\partial v} + \frac{\partial p}{\partial v}) - (\xi\;pp - 4x + p)(\xi\;\frac{\partial rt}{\partial v} - \frac{\partial crct}{\partial v})}{(\xi\;rt - crct)^2}$$
$$\frac{\partial \xi}{\partial v} = 0.0$$

Table 1. Sensitivity of flutter speed with respect to various parameters (M=0.85)
($\mu = 100$, $x_\theta = 0.25$, $r_\theta = 0.5$, $\omega_h = 10$ rad/s.,
$\omega_\theta = 50$ rad/s., $b = 5$ in., $a_h = -0.5$)

Parameter	Analytic derivative	Finite Difference derivative		
		1%[a]	0.1%	0.01%
μ	0.39296	0.38798	0.39244	0.39289
x_θ	-253.60673	-248.75989	-253.10277	-253.54363
r_θ	239.41460	236.53840	239.11255	239.37244
ω_h	-4.35016	-4.31603	-4.34651	-4.34958
ω_θ	2.71689	2.68798	2.71383	2.71644

[a] indicates step size

Table 2. Sensitivity of flutter speed with respect to various parameters at different transonic Mach numbers
($\mu = 100$, $x_\theta = 0.25$, $r_\theta = 0.5$, $\omega_h = 10$ rad/s., $\omega_\theta = 50$ rad/s., $b = 5$ in., $a_h = -0.5$)

Parameter	Mach number	Sensitivity derivatives		
		Analytic	Finite Difference	
			0.1%[b]	0.01%
μ	0.8	0.44303	0.44247	0.44298
	0.85	0.39296	0.39244	0.39289
	0.8625	0.46202	0.46143	0.46196
	0.87	0.53132	0.53010	0.53070
x_θ	0.8	-241.52263	-241.07122	-241.47758
	0.85	-253.60673	-253.10277	-253.54363
	0.8625	-463.70394	-462.54019	-463.58734
	0.87	-734.98634	-731.92101	-733.99406
r_θ	0.8	243.06012	242.76615	243.03092
	0.85	239.41460	239.11255	239.37244
	0.8625	308.46665	308.08430	308.42838
	0.87	391.63750	390.75475	391.18409
ω_h	0.8	-3.78605	-3.78311	-3.78576
	0.85	-4.35016	-4.34651	-4.34958
	0.8625	-6.90676	-6.90064	-6.90615
	0.87	-10.17027	-10.14904	-10.15867
ω_θ	0.8	2.80282	2.79985	2.80253
	0.85	2.71689	2.71383	2.71644
	0.8625	3.58044	3.57671	3.58007
	0.87	4.60379	4.59453	4.59857

[b] denotes step size

Table 3. Comparison of natural frequencies of an unswept wing
($Area = 0.02318\ m^2$, $Aspect\ ratio = 4.0132$, $Taper\ ratio = 1.0$)
for different laminate sequences

Laminate sequence	Natural frequencies (Hz.)					
	Present			Landsberger and Dugundji [36]		
	First	Second	Third	First	Second	Third
$[0_2/90]_s$	11.03	39.30	69.06	10.8	39	67
$[15_2/0]_s$	8.86	42.62	63.25	8.5	48	58
$[\pm 15/0]_s$	10.12	48.9	64.94	9.9	50	63
$[+30_2/0]_s$	6.21	37.57	57.78	6.0	41	60
$[\pm 30/0]_s$	7.73	48.76	64.42	7.8	50	65

Table 4. Comparison of flutter speed of an unswept wing
($Area = 0.02318\ m^2$, $Aspect\ ratio = 4.0132$, $Taper\ ratio = 1.0$)
in subsonic flow

Laminate sequence	Flutter speed (m/s)	
	Present	Experimental [36]
$[0_2/90]_s$	24.9	26
$[15_2/0]_s$	23.2	25
$[\pm 15/0]_s$	28.1	28
$[\mp 15/0]_s$	18.9	21
$[+30_2/0]_s$	28.8	29

Table 5. Comparison of natural frequencies of the 2.5 foot WEAK3 model ($Area = 3.782\ ft^2$, $Aspect\ ratio = 1.6525$, $Taper\ ratio = 0.6576$, $Sweep = 45^o$) with measured values

Natural frequencies (Hz.)	Present	Experimental [37]
First	9.91	9.60
Second	36.75	38.10
Third	60.78	50.70
Fourth	102.11	98.50

Table 6. Comparison of flutter speed of the 2.5 foot WEAK3 model ($Area = 3.782\ ft^2$, $Aspect\ ratio = 1.6525$, $Taper\ ratio = 0.6576$, $Sweep = 45^o$) with flutter data measured in the transonic wind tunnel

Mach number M	Mass ratio μ	Density of air $(slugs/ft^3)$	Flutter speed, V (ft/s)	Non-dimensional speed $(V/b_s\omega_\alpha\sqrt{\mu})$	
				Present	Experimental [37]
0.499	33.465	0.000830	476.90	0.3896	0.4459
0.678	68.753	0.000404	640.00	0.3647	0.4174
0.901	143.92	0.000193	829.44	0.3267	0.3700

Table 7. Sensitivity of divergence speed of the wing at M=0.9
($Area = 20\ m^2$, $Aspect\ ratio = 10$, $Taper\ ratio = 0.5$)
with respect to shape parameters

Sweep angle (deg)	Divergence speed(m/s)	Parameter	Analytic derivative	Finite difference derivative		
				1.0%[a]	0.1%	0.01%
0	137.41	Aspect ratio	-4.9672	-4.9276	-4.9630	-4.9642
		Area	-4.2460	-4.2156	-4.2418	-4.2433
		Taper ratio	7.2069	7.4086	7.2601	7.2308
		Sweep angle	147.0488	147.1087	147.2050	148.5662
15	203.74	Aspect ratio	16.9889	17.4989	17.0278	16.9773
		Area	-18.3916	-17.9050	-18.3307	-18.3768
		Taper ratio	440.3419	451.3756	441.1370	440.0515
		Sweep angle	434.5355	437.5666	434.5507	434.0796

[a] indicates step size

Table 8. Sensitivity of flutter speed of the wing at M=0.9
($Area = 20\ m^2$, $Aspect\ ratio = 10$, $Taper\ ratio = 0.5$)
with respect to shape parameters

Sweep angle (deg)	Flutter speed(m/s)	Parameter	Analytic derivative	Finite difference derivative	
				0.1%[a]	0.01%
0	229.90	Aspect ratio	-12.6812	-12.6675	-12.6779
		Area	-6.4607	-6.4563	-6.4592
		Taper ratio	-184.8167	-184.7288	-184.7691
		Sweep angle	-104.4327	-104.3587	-104.4143
15	209.67	Aspect ratio	-10.1067	-10.0929	-10.1005
		Area	-4.3196	-4.3181	-4.3170
		Taper ratio	-199.1987	-199.1011	-199.0925
		Sweep angle	-37.7435	-37.6769	-37.5526
30	213.22	Aspect ratio	-6.6440	-6.6311	-6.6404
		Area	-5.0568	-5.0542	-5.0554
		Taper ratio	-172.6965	-172.6105	-172.6414
		Sweep angle	67.8415	67.9632	67.8975

[a] indicates step size

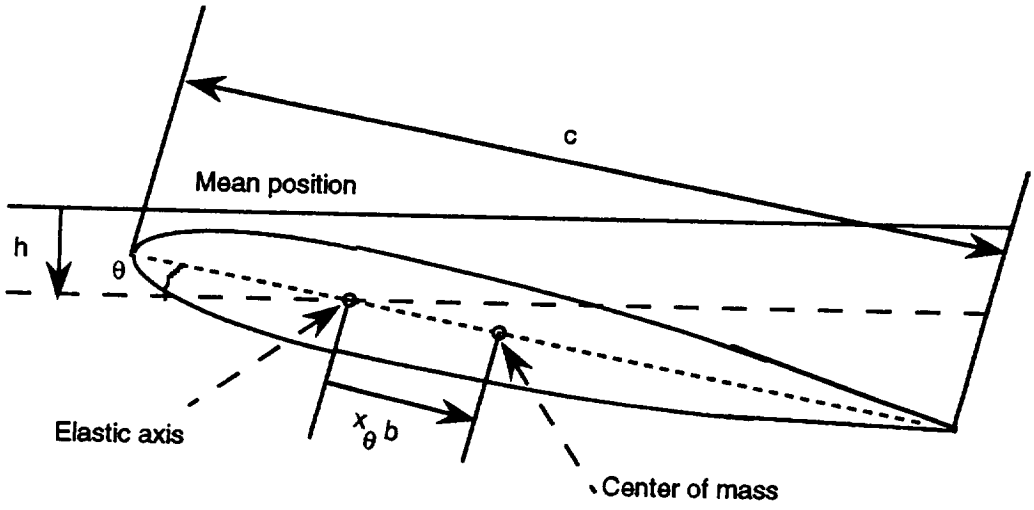

Fig 1. Two degree of freedom airfoil

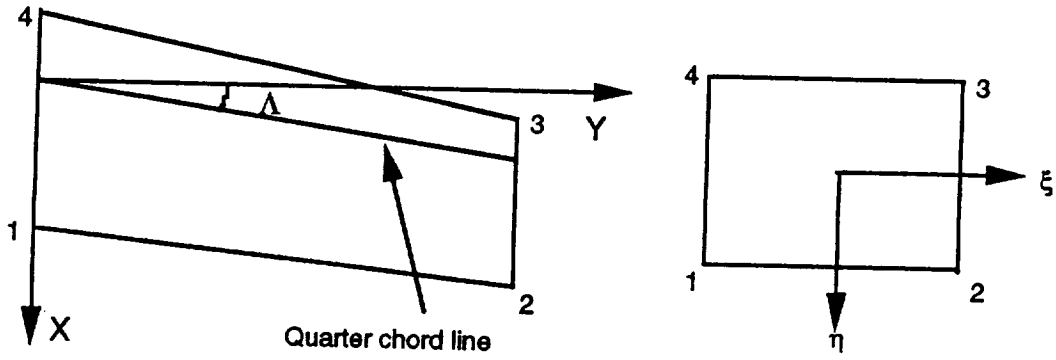

Fig 2. Original and Transformed Coordinate Systems

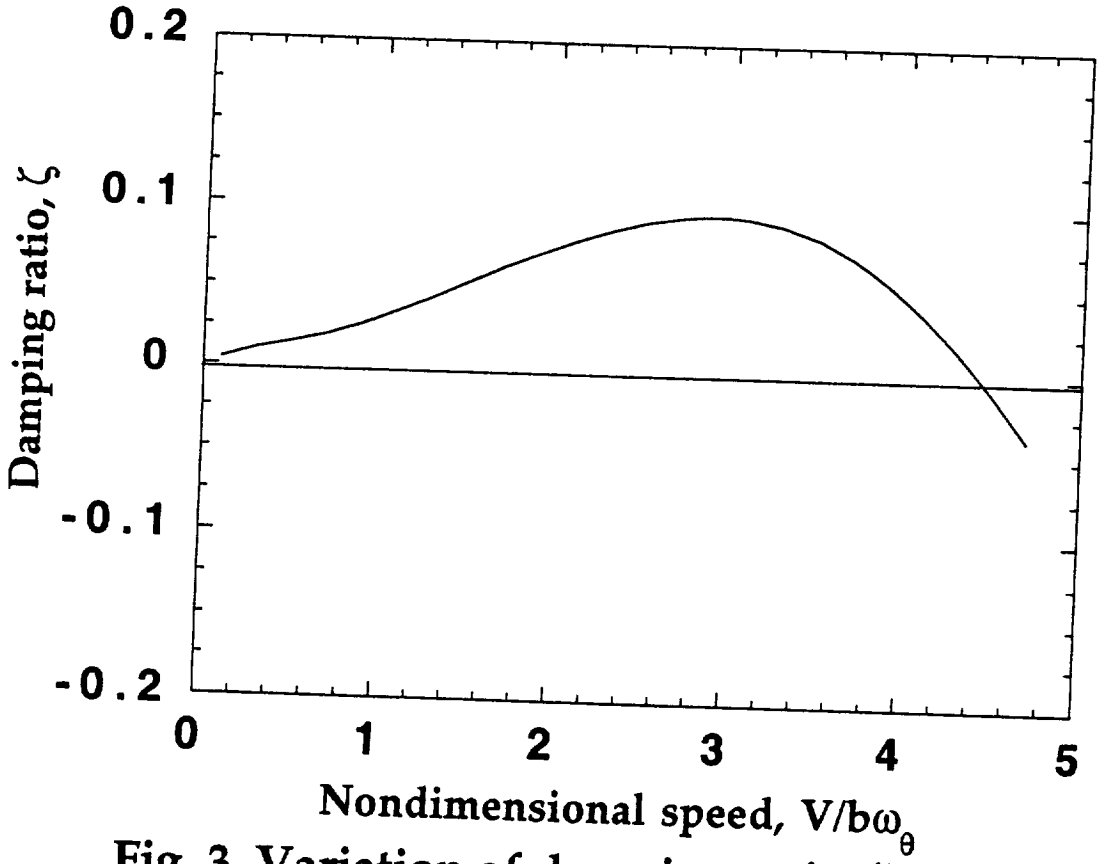

Fig. 3 Variation of damping ratio, ζ with nondimensional speed, $V/b\omega_\theta$

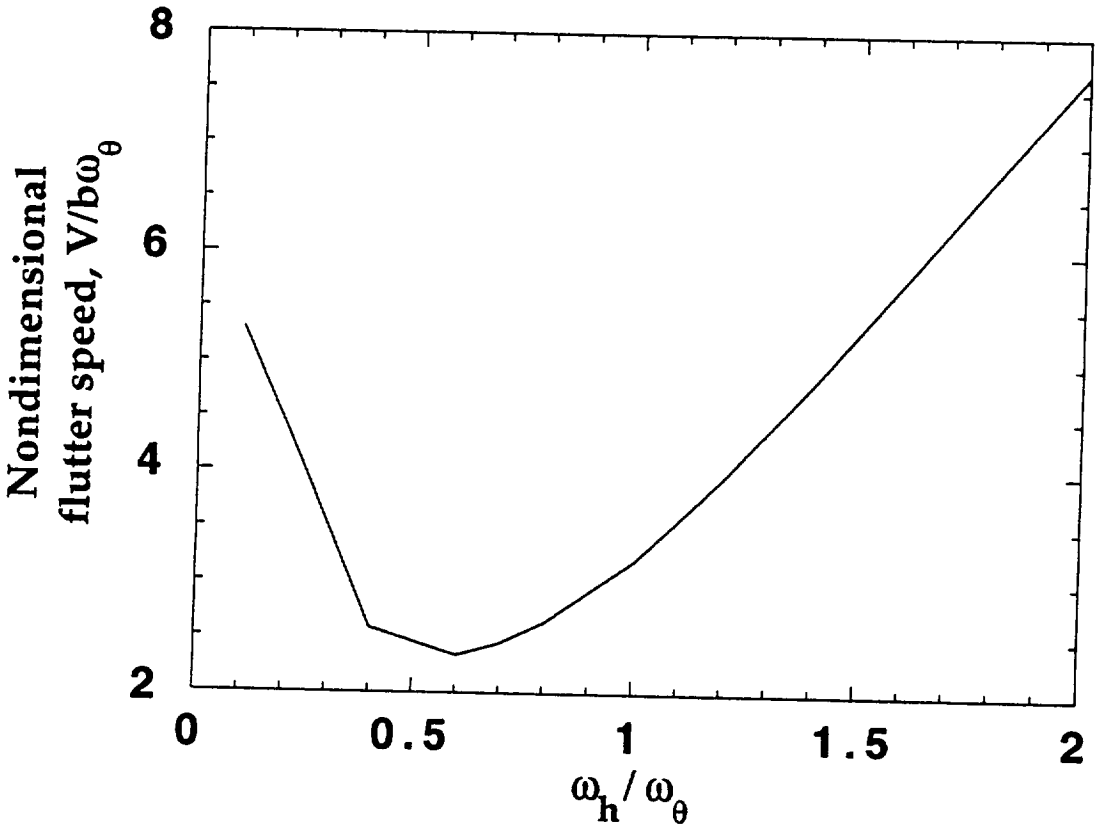

Fig. 4 Variation of nondimensional speed, $V/b\omega_\theta$ with ratio of frequencies, ω_h/ω_θ

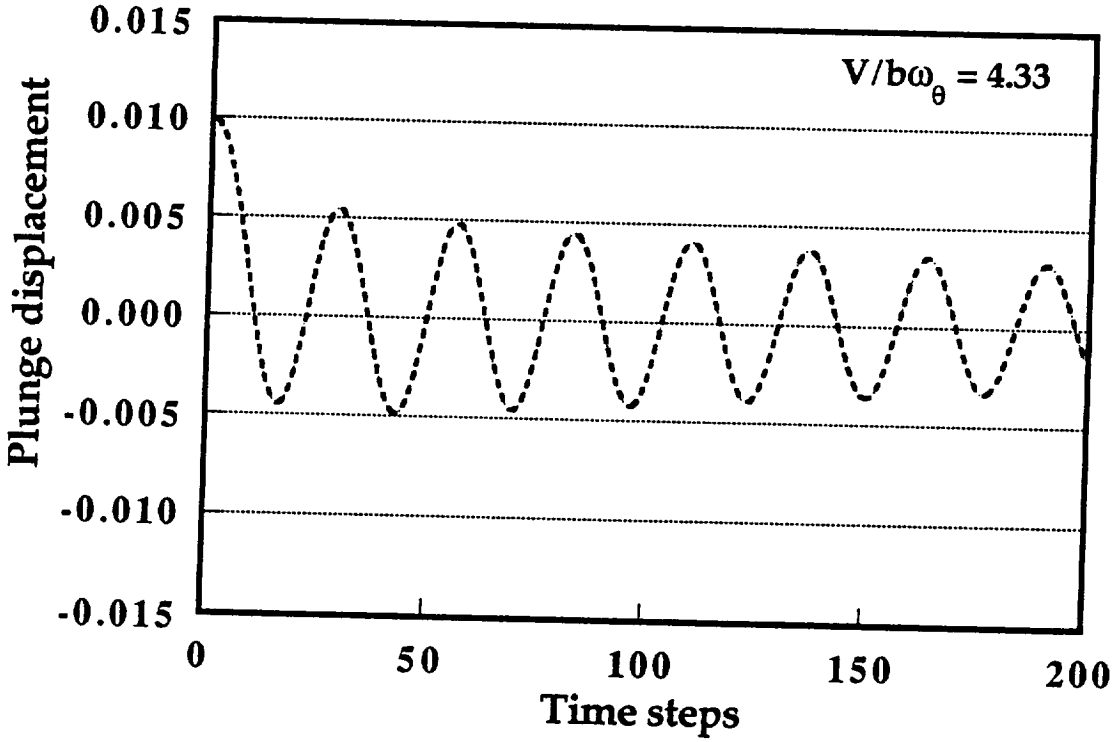

Fig. 5a Plunge displacement Vs time
(1 time step = 0.01 sec.)

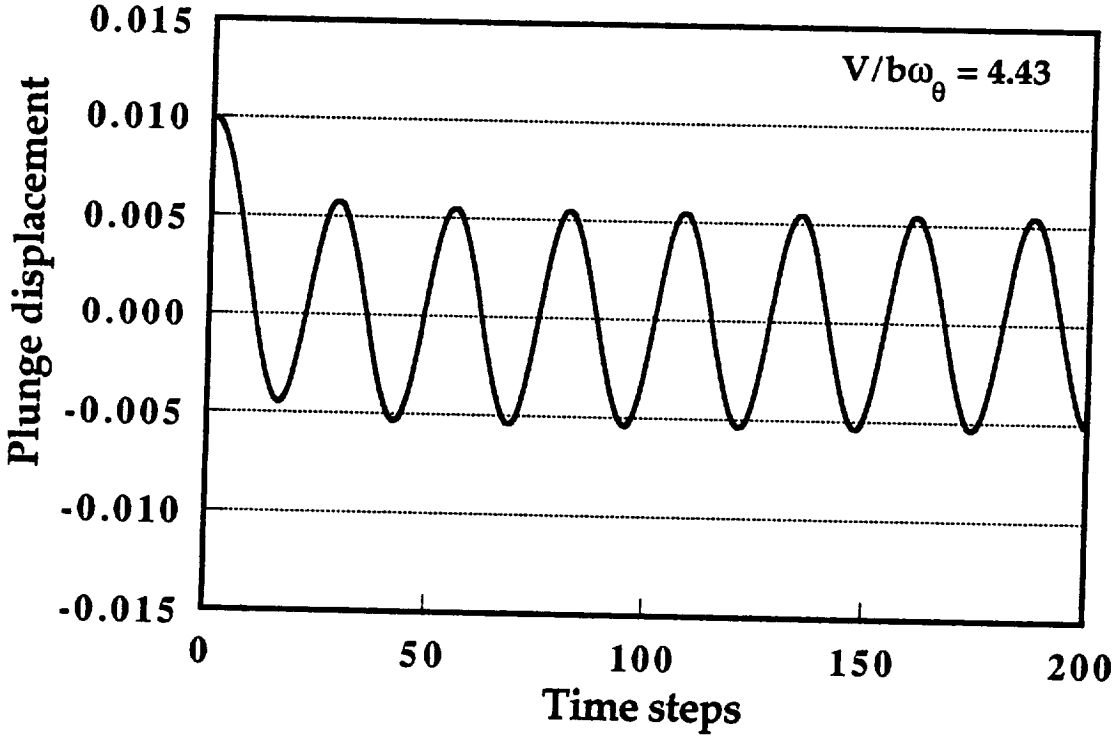

Fig. 5b Plunge displacement Vs time
(1 time step = 0.01 sec.)

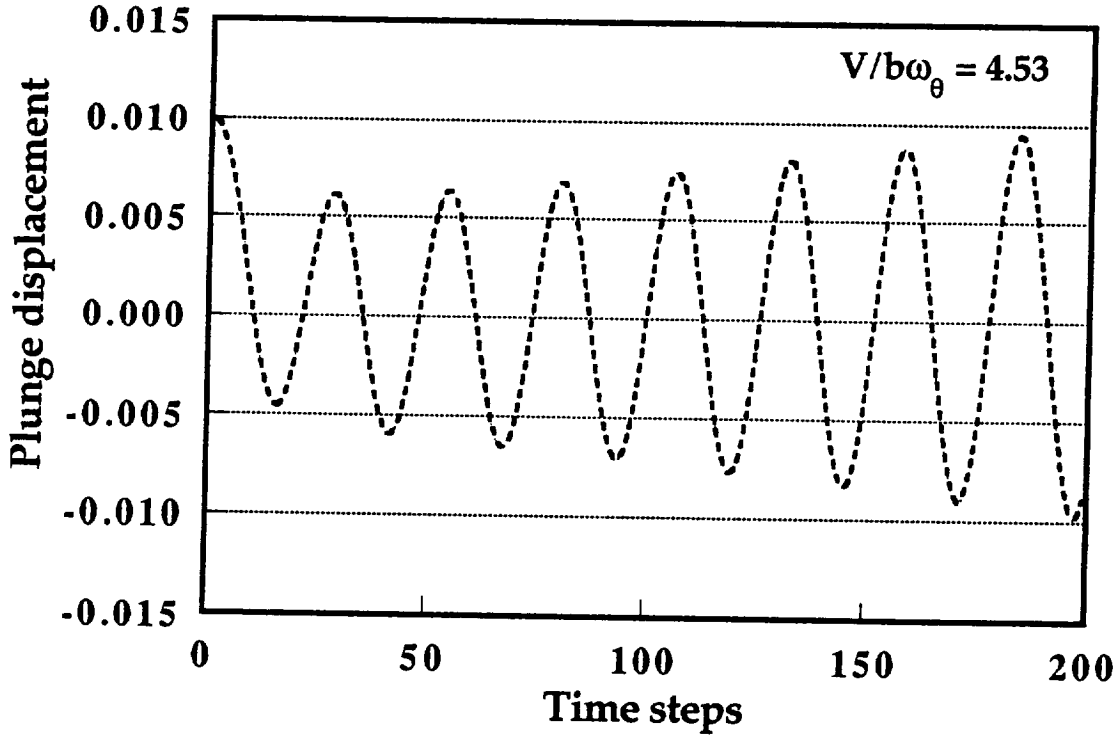

Fig. 5c Plunge displacement Vs time
(1 time step = 0.01 sec.)

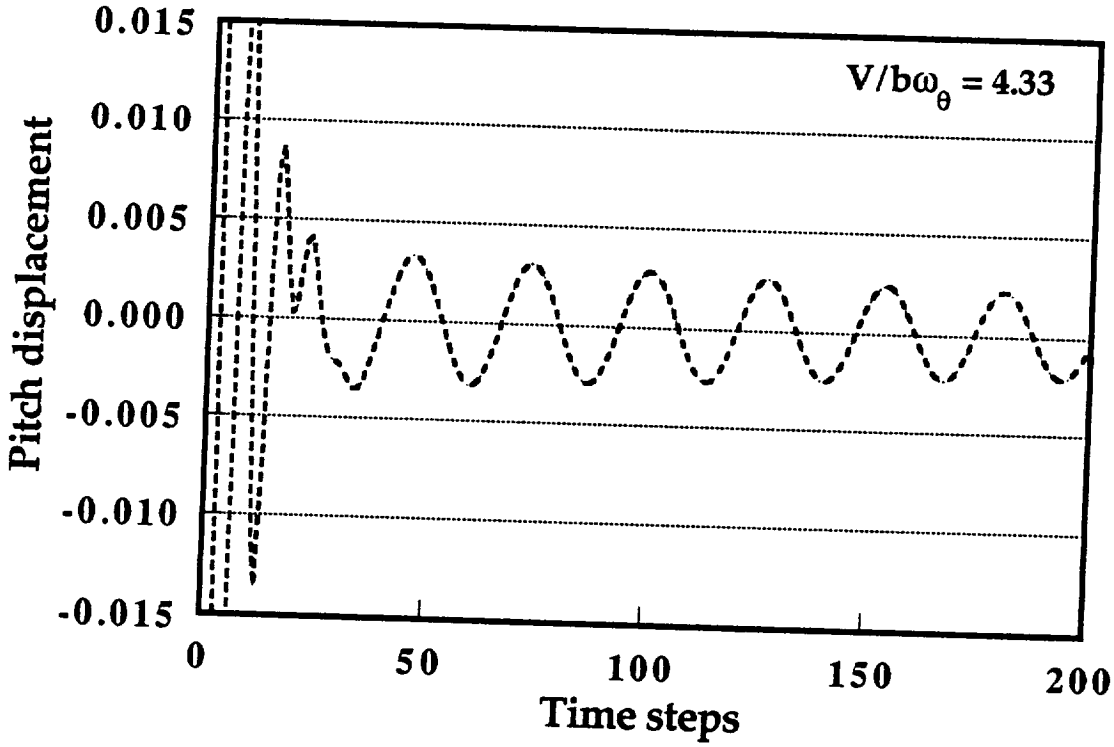

Fig. 6a Pitch displacement Vs time
(1 time step = 0.01 sec.)

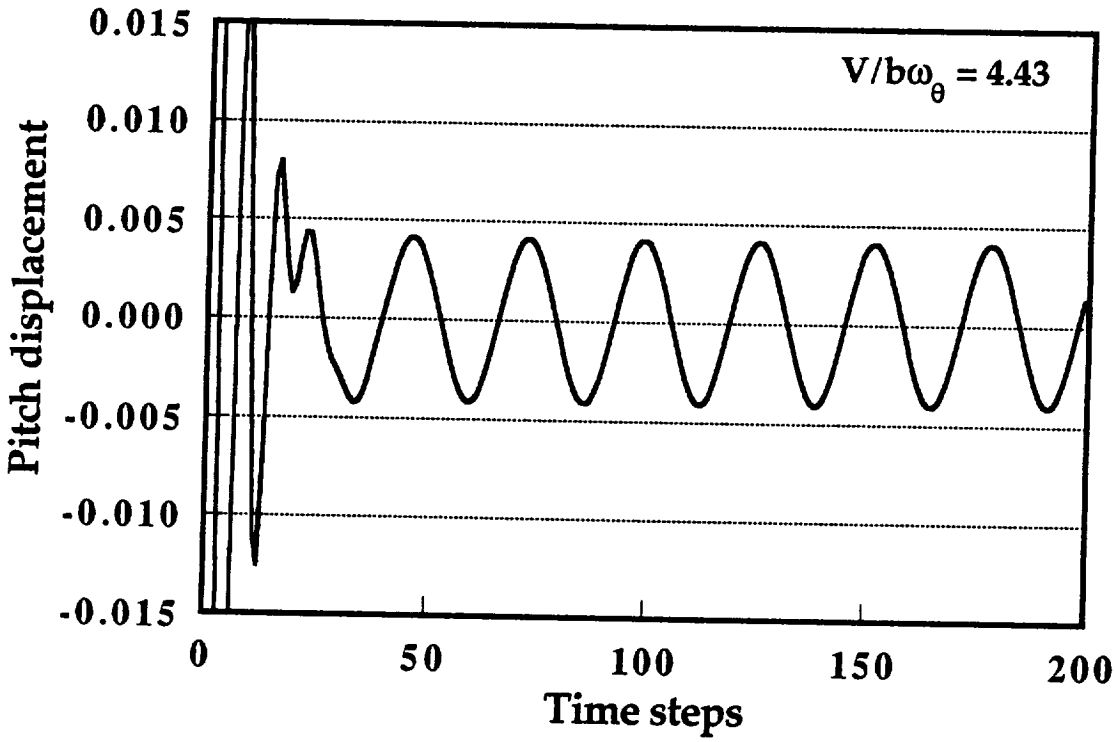

Fig. 6b Pitch displacement Vs time
(1 time step = 0.01 sec.)

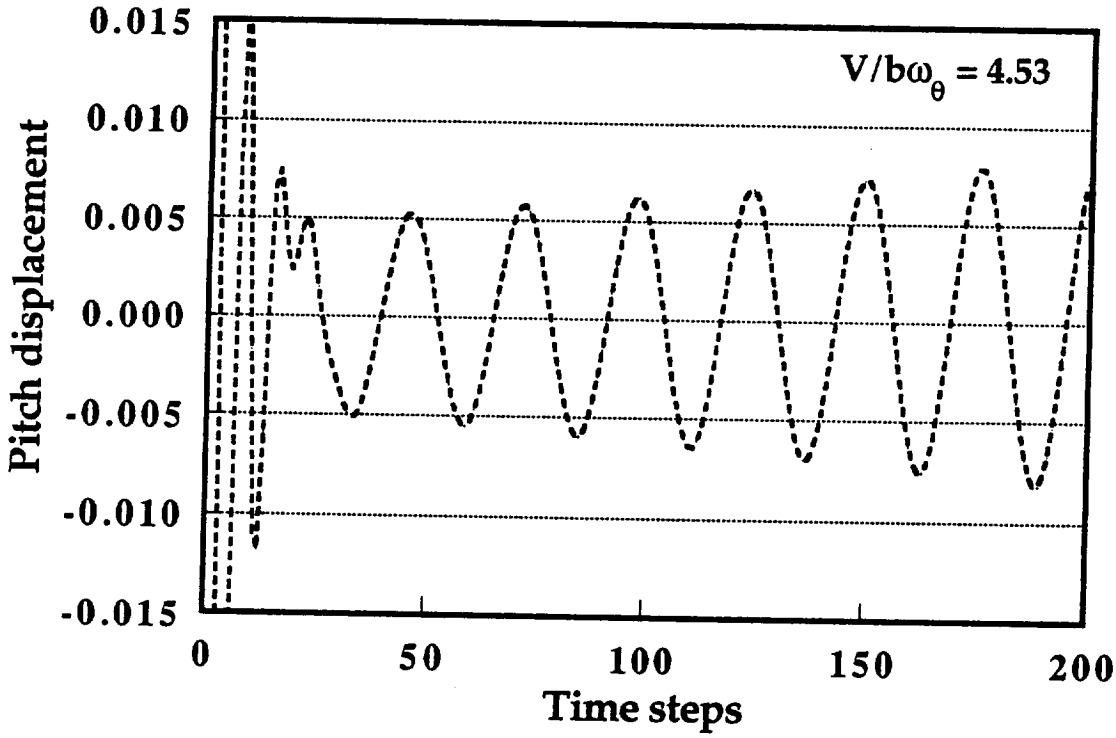

Fig. 6c Pitch displacement Vs time
(1 time step = 0.01 sec.)

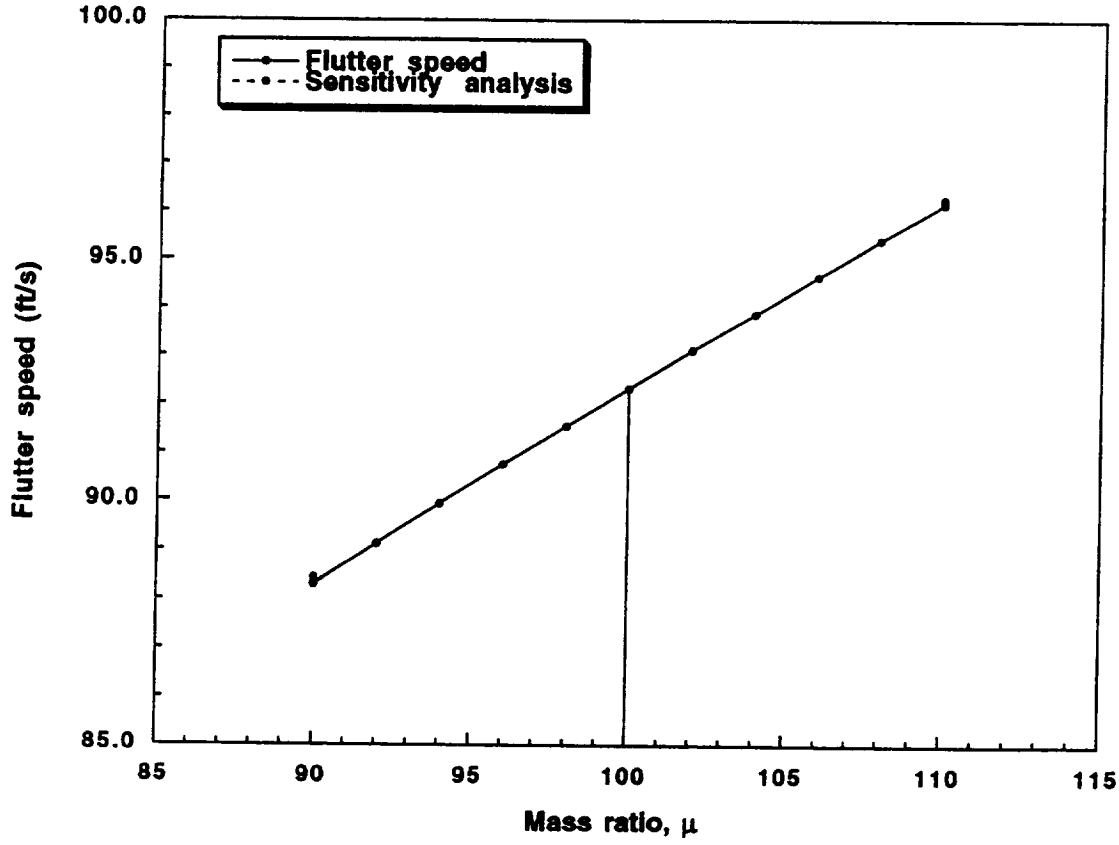

Fig. 7 Flutter speed Vs Mass ratio

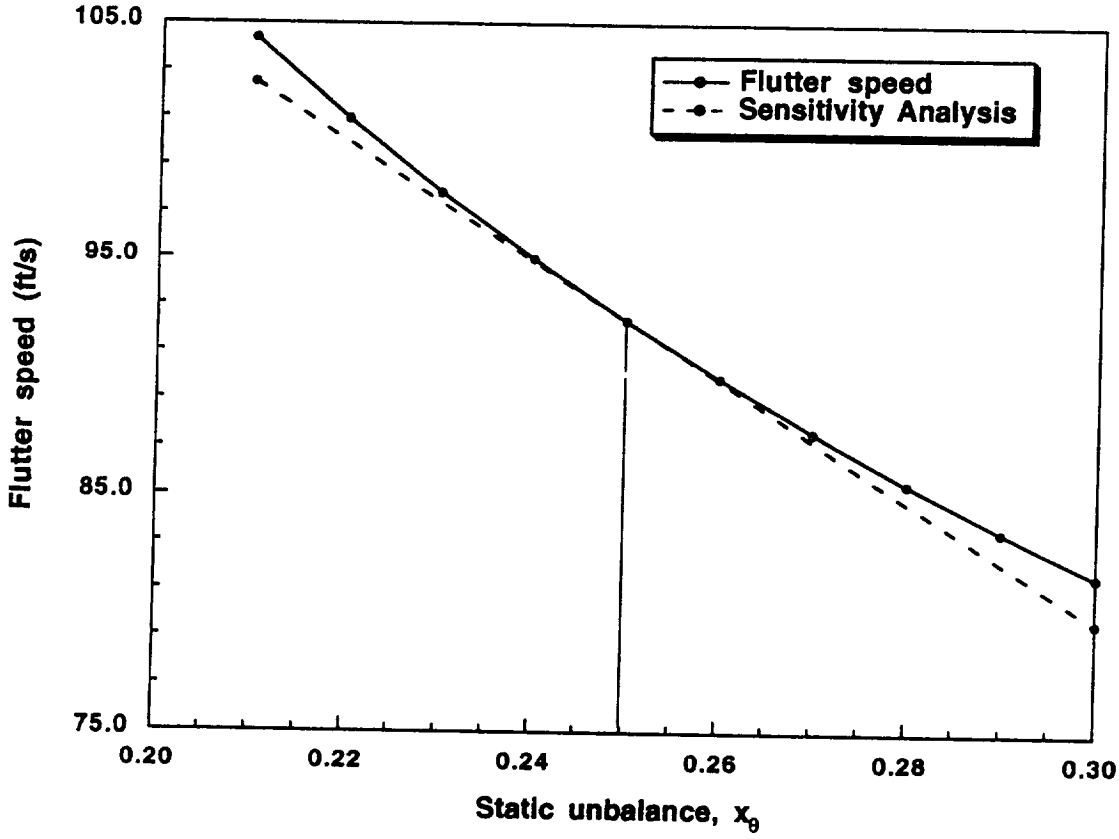

Fig. 8 Flutter speed Vs Static unbalance

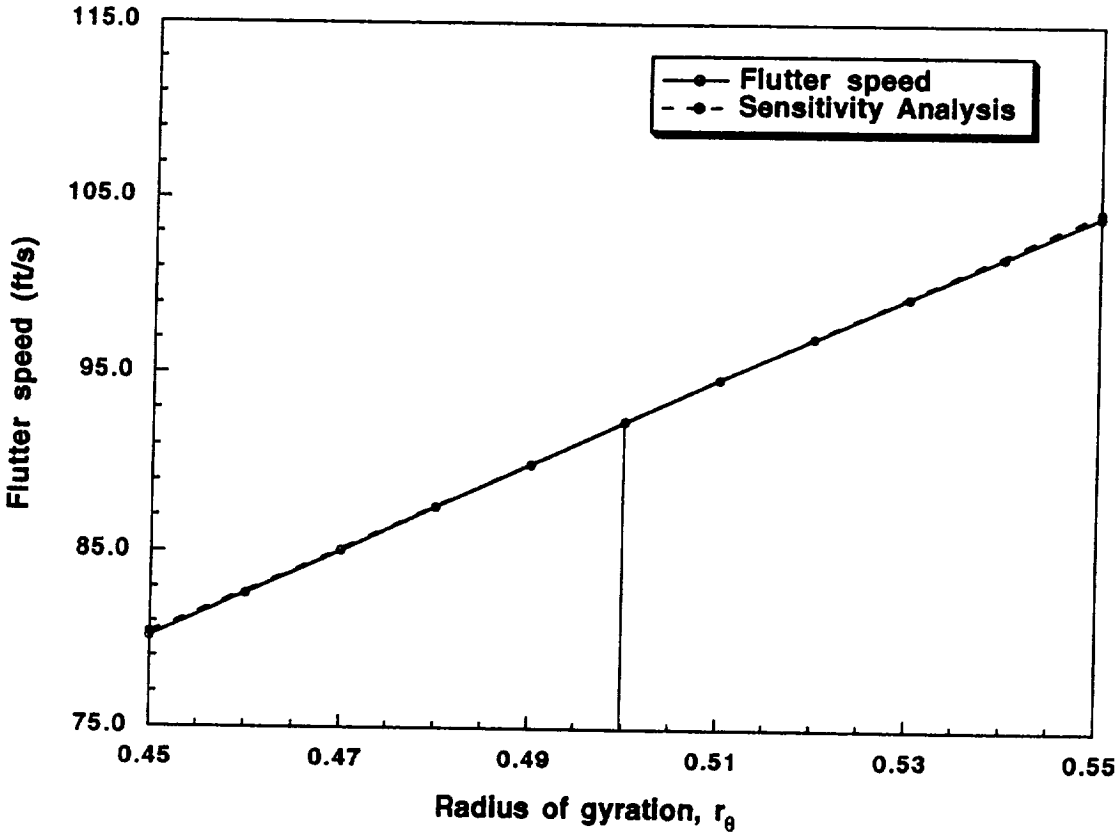

Fig. 9 Flutter speed Vs Radius of gyration

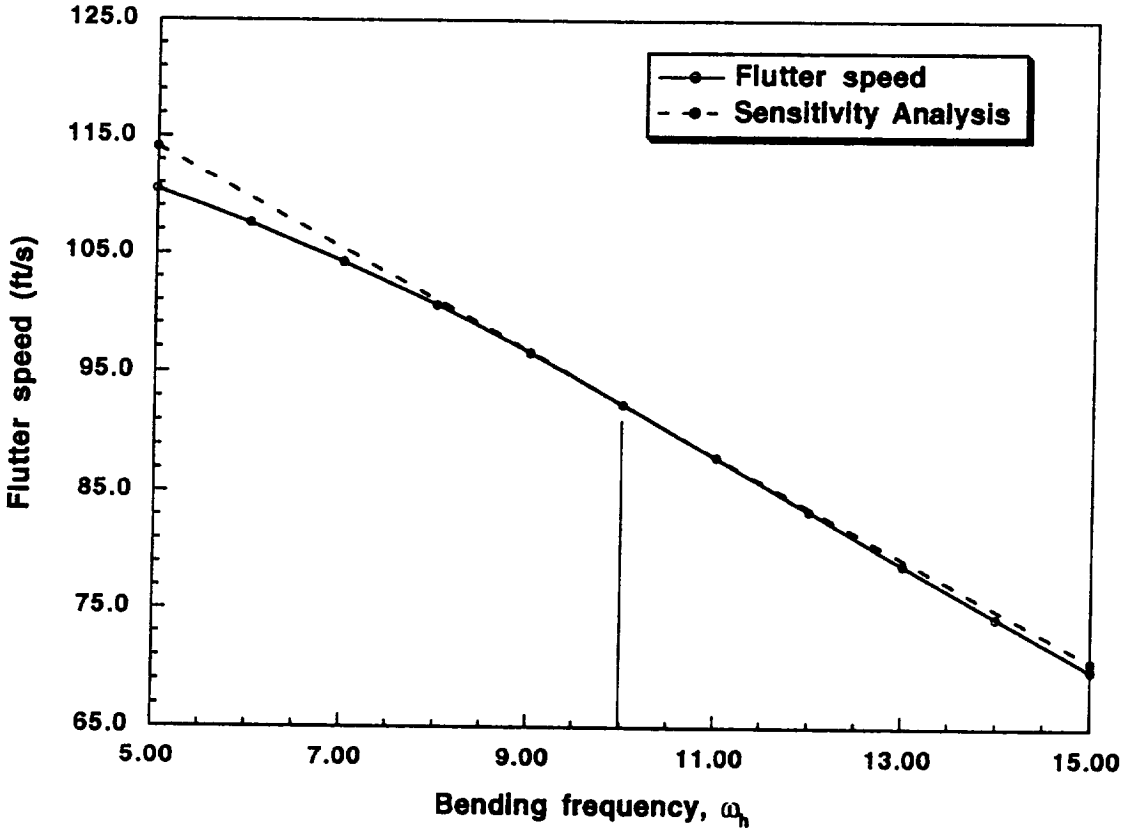

Fig. 10 Flutter speed Vs Bending frequency

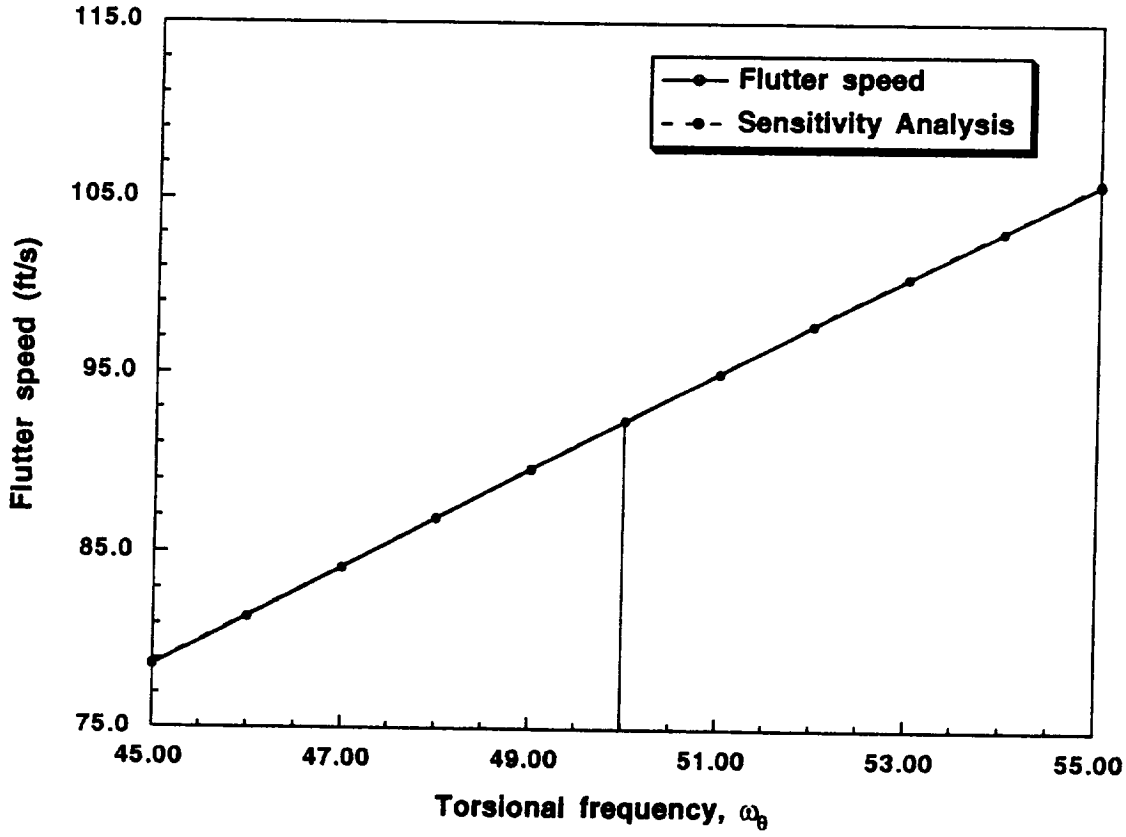

Fig. 11 Flutter speed Vs Torsional frequency

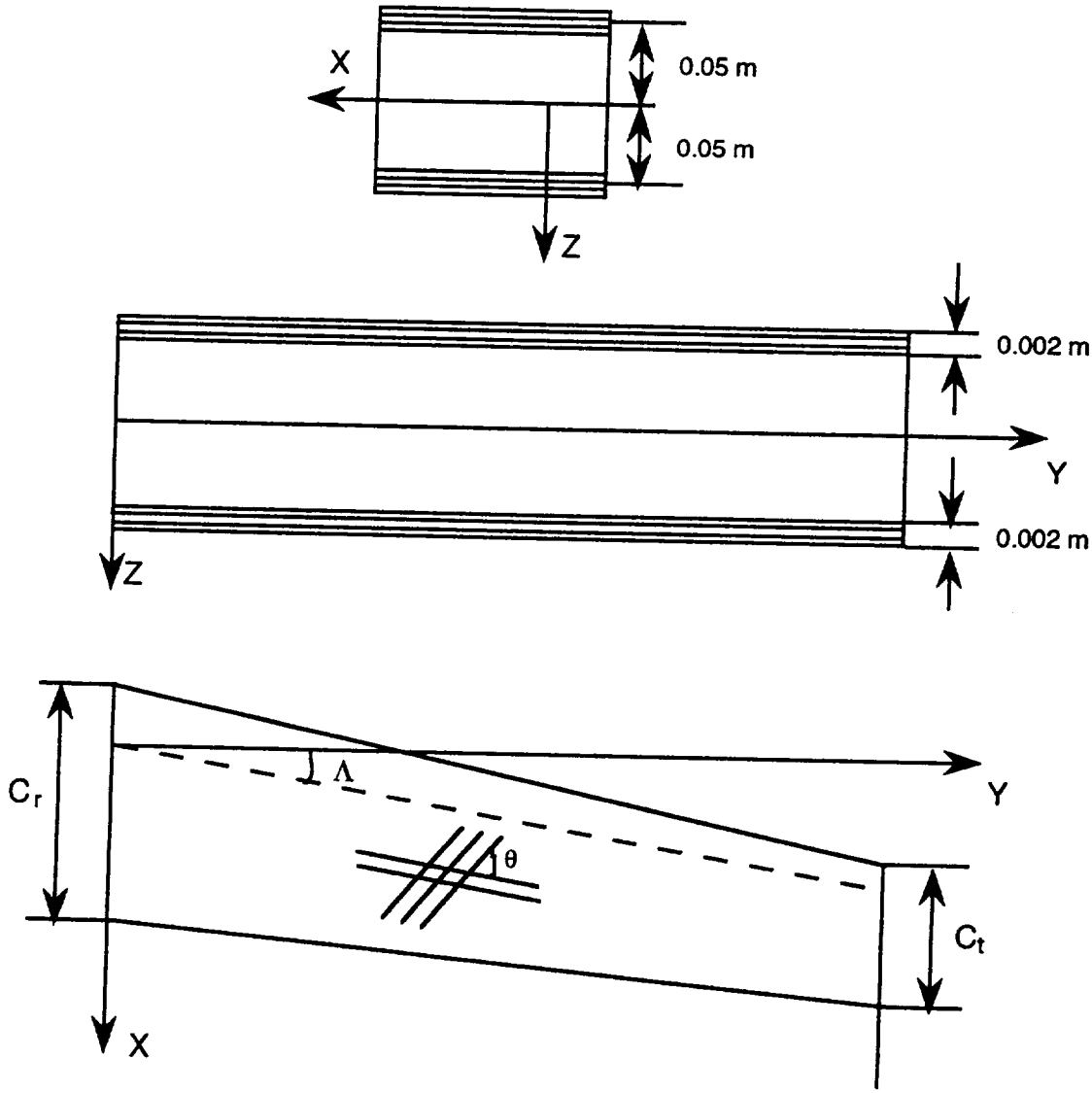

Fig 12. Wing box section used

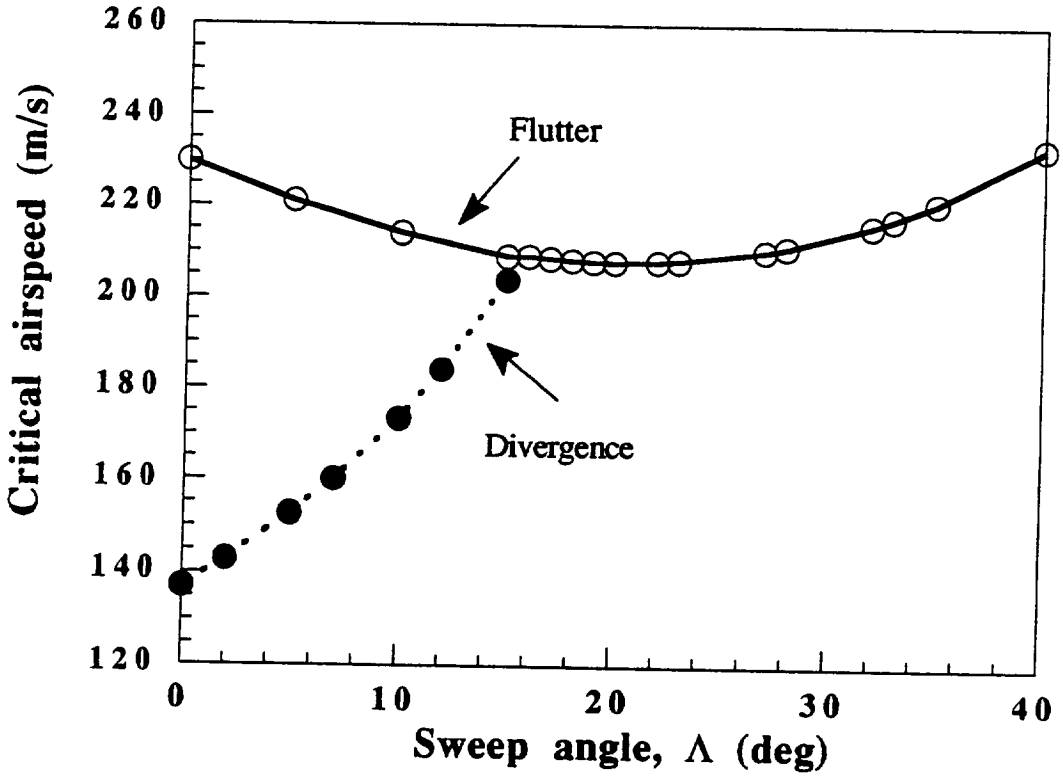

Fig. 13 Critical speed Vs Sweep Angle
(AR=10, Area=20 m^2, TR=0.5)

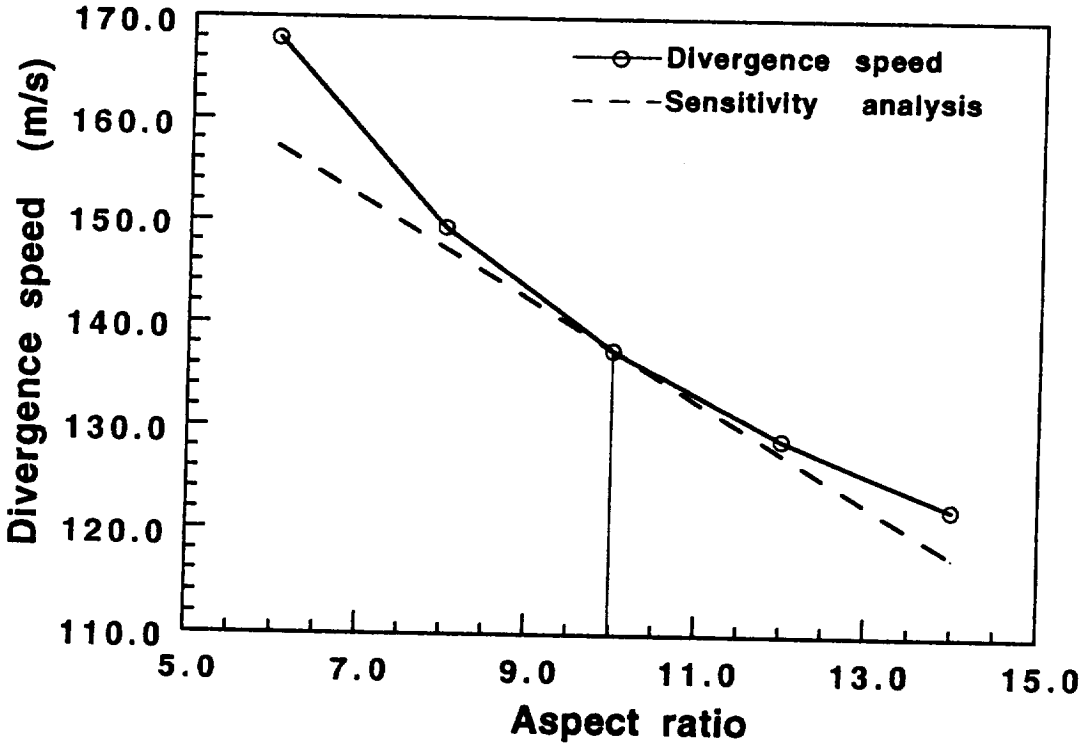

Fig 14. Divergence speed Vs Aspect ratio (M=0.9)
(AR=10, Area=20m^2, TR=0.5, Sweep=0^o)

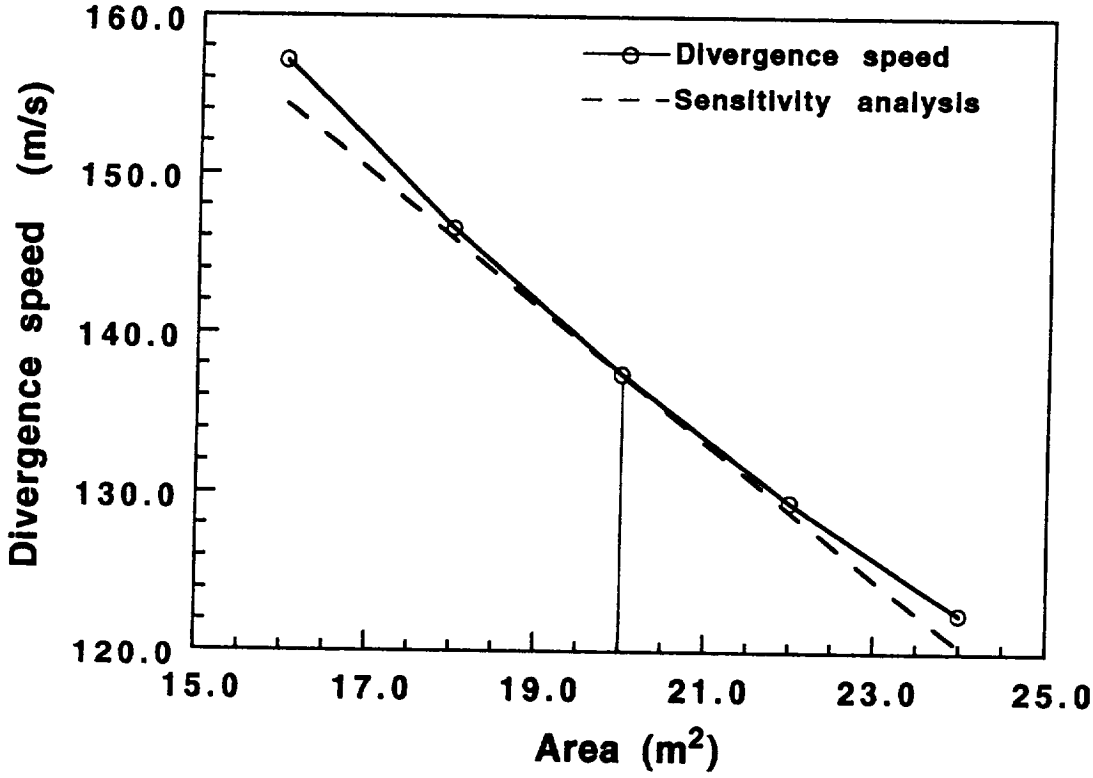

Fig 15. Divergence speed Vs Area (M=0.9)
(AR=10, Area=20m², TR=0.5, Sweep=0°)

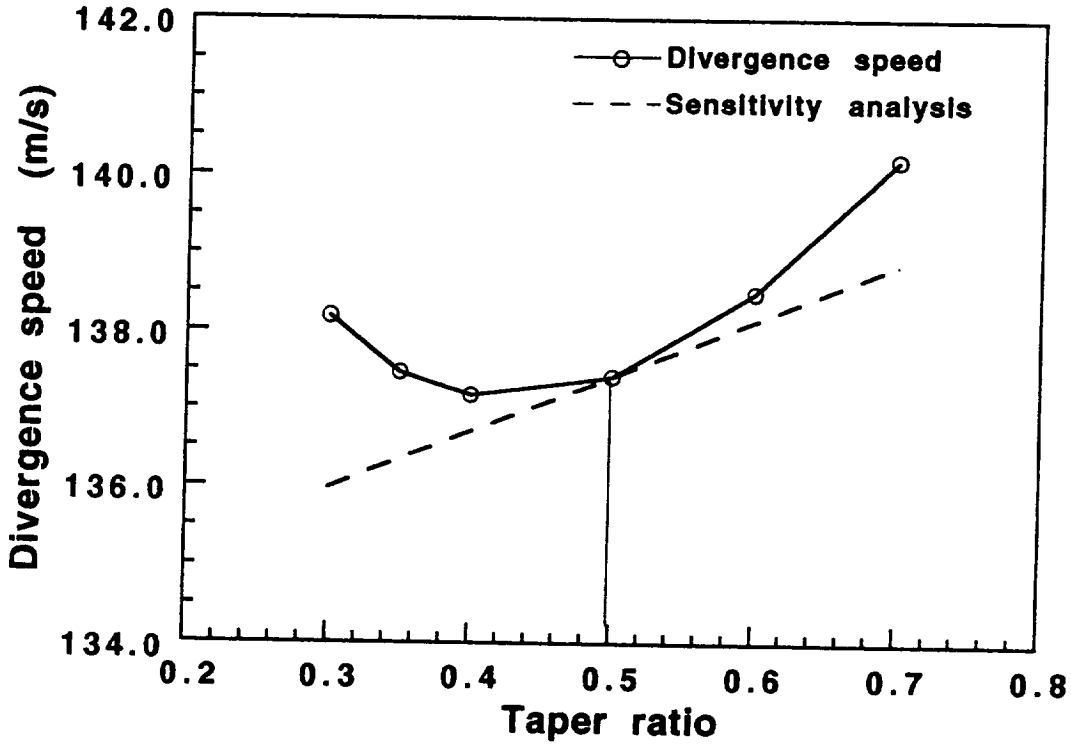

Fig 16. Divergence speed Vs Taper ratio (M=0.9)
(AR=10, Area=20m^2, TR=0.5, Sweep=0^o)

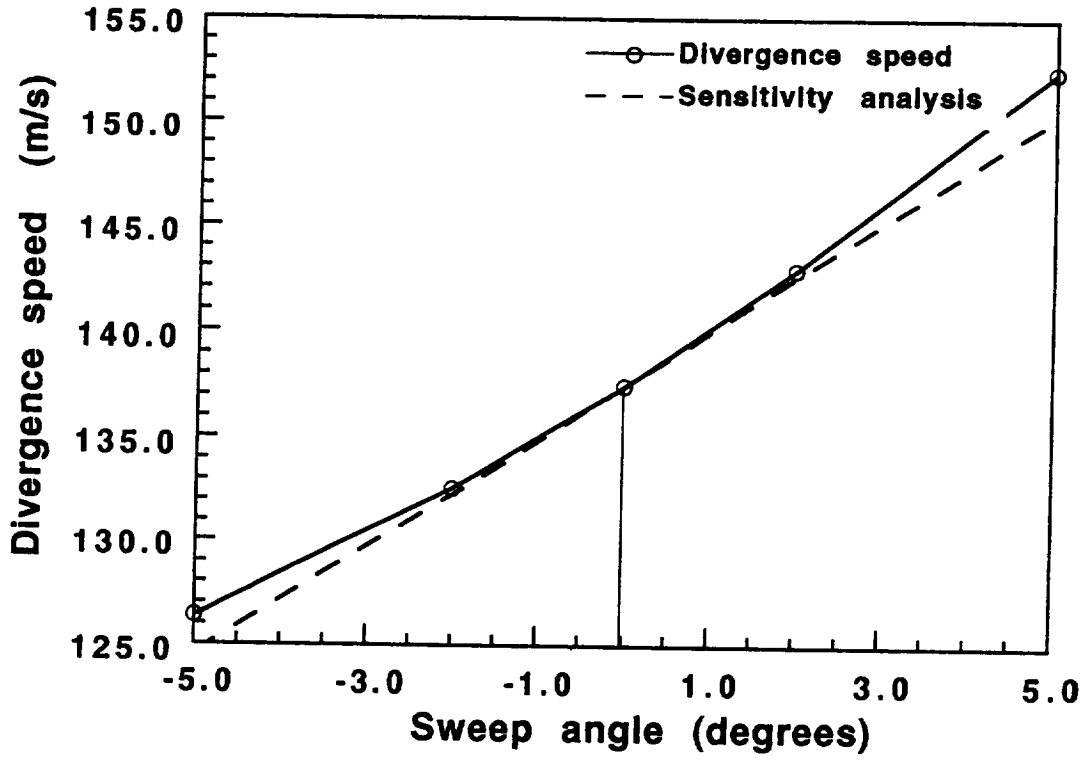

Fig 17. Divergence speed Vs Sweep angle (M=0.9)

(AR=10, Area=20m^2, TR=0.5, Sweep=0^o)

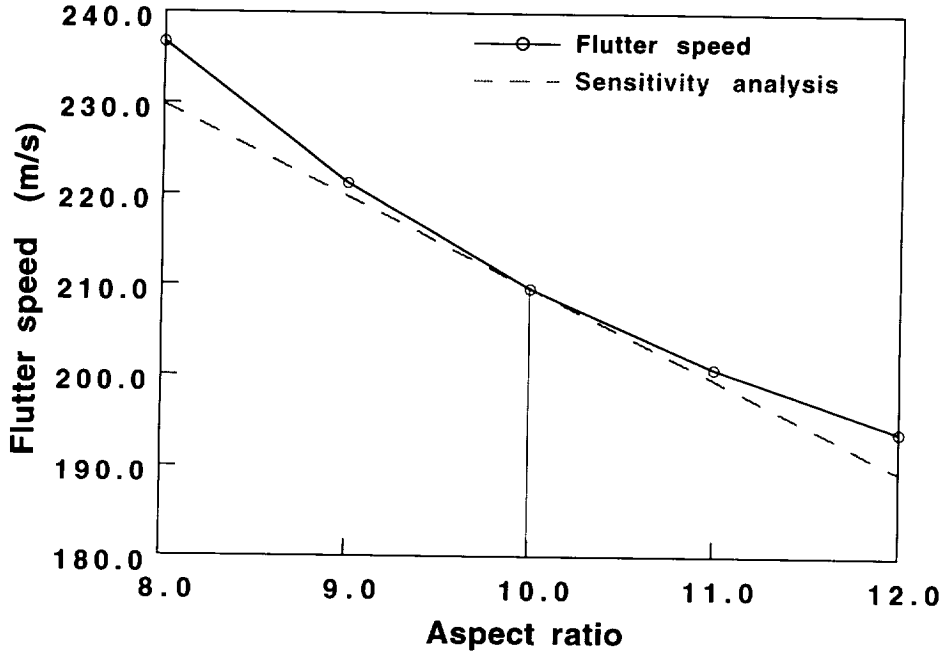

Fig 18. Flutter speed Vs Aspect ratio (M=0.9)
(AR=10, Area=20m², TR=0.5, Sweep=15°)

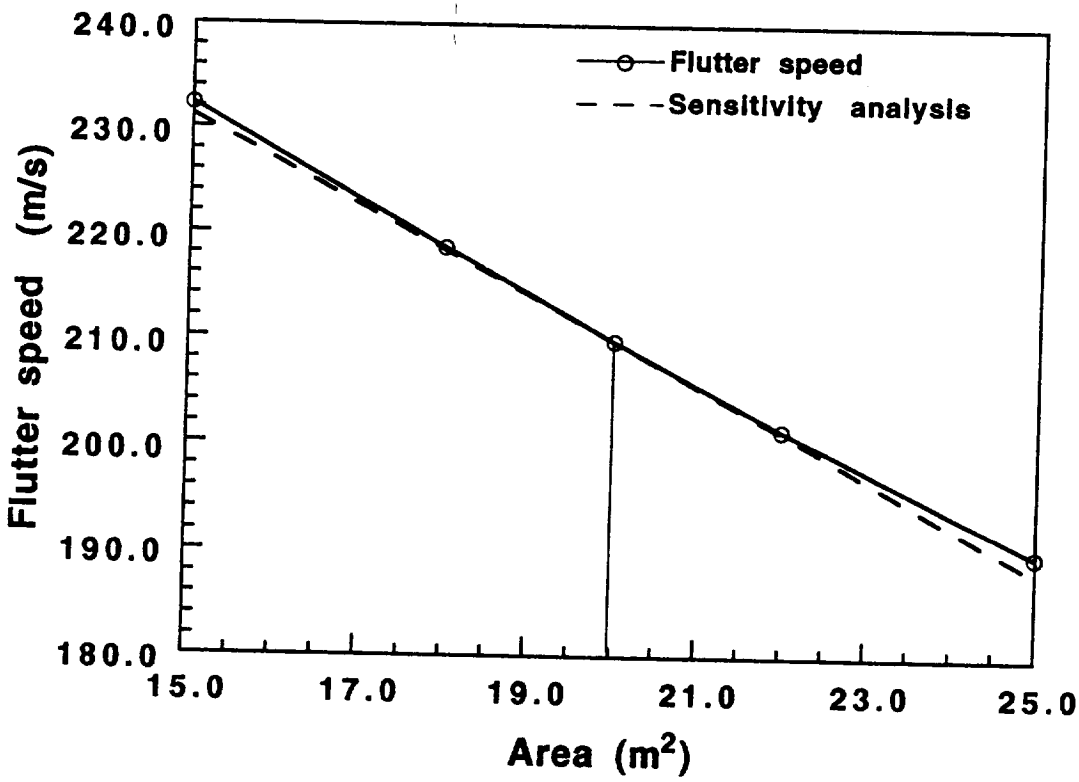

Fig 19. Flutter speed Vs Area (M=0.9)

(AR=10, Area=20m², TR=0.5, Sweep=15°)

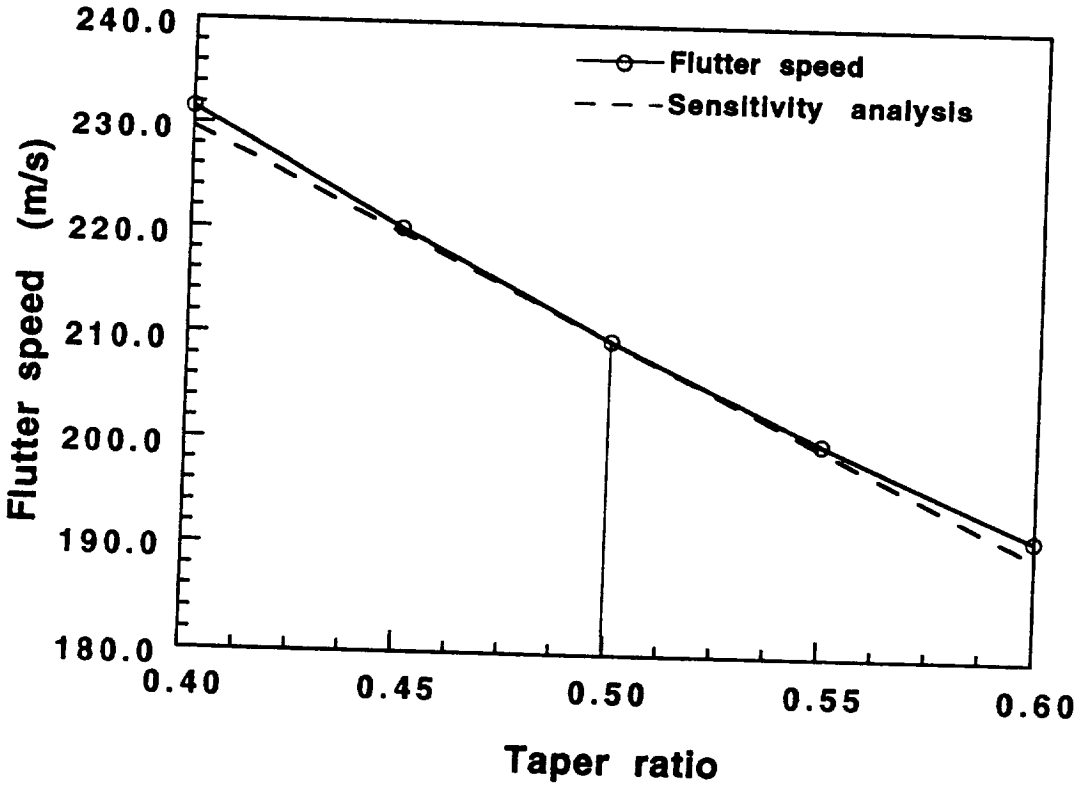

Fig 20. Flutter speed Vs Taper ratio (M=0.9)
(AR=10, Area=20m^2, TR=0.5, Sweep=15^o)

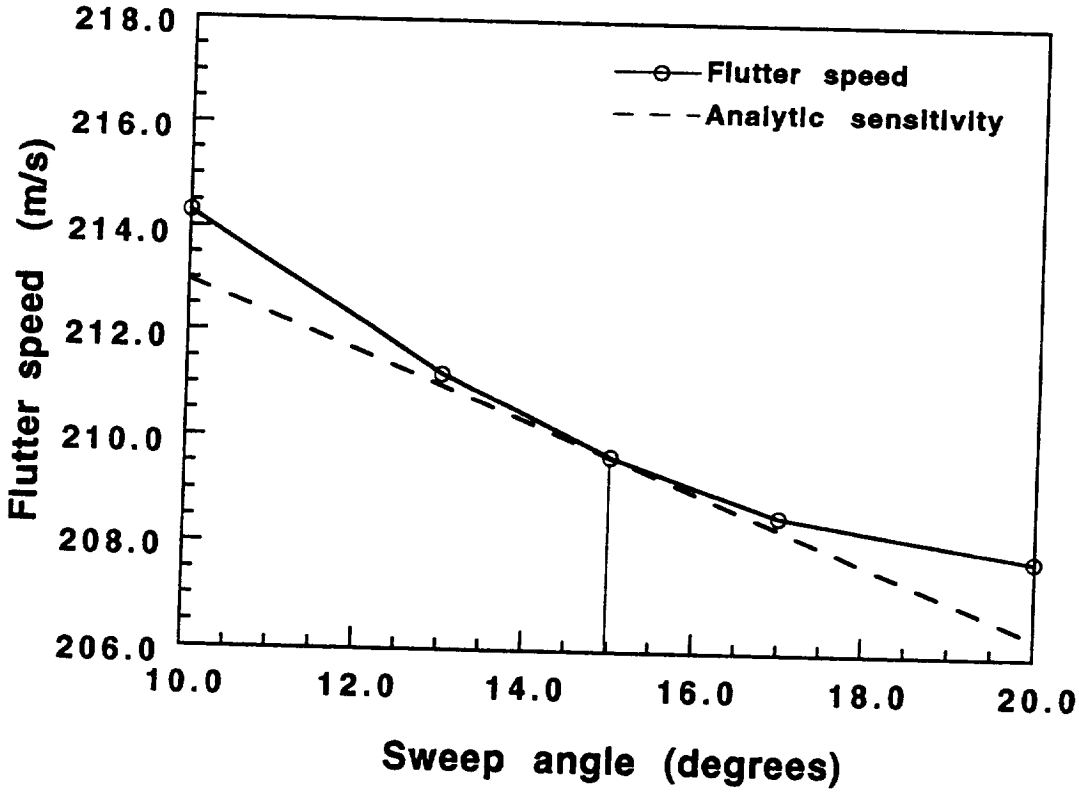

Fig 21. Flutter speed Vs Sweep angle (M=0.9)
(AR=10, Area=20m^2, TR=0.5, Sweep=15^o)

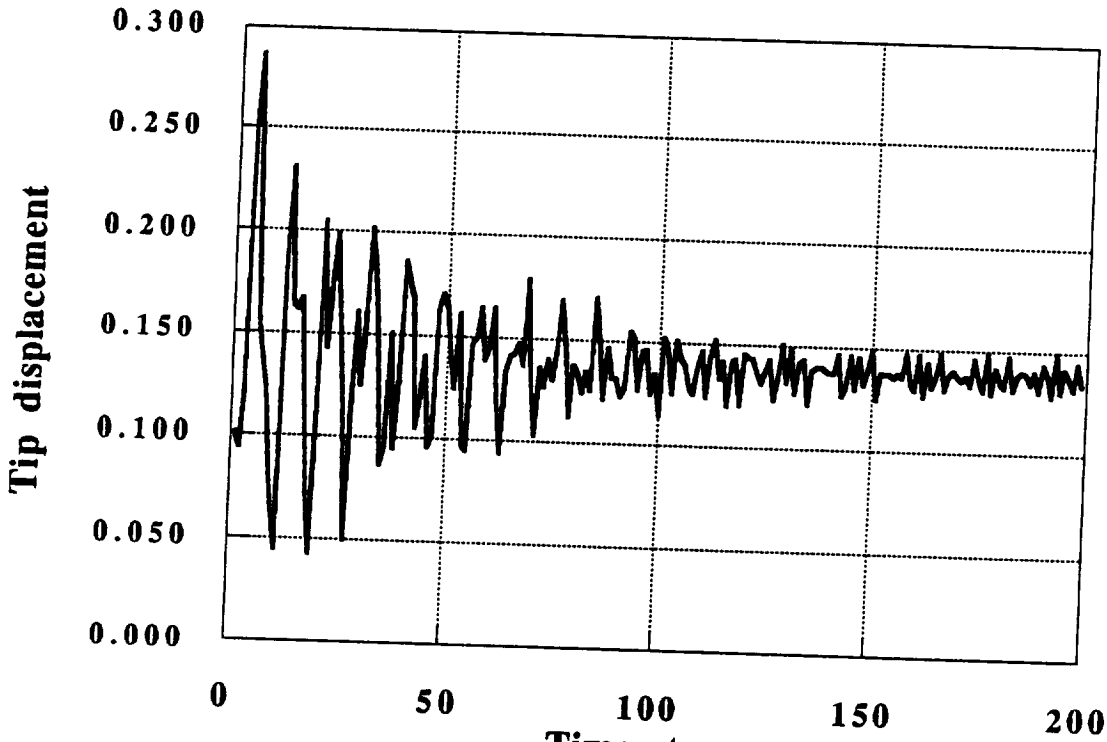

Fig 22. Displacement Vs Time at V=137.41 m/s

(AR=10, Area=20m^2, TR=0.5, Sweep=0^o)

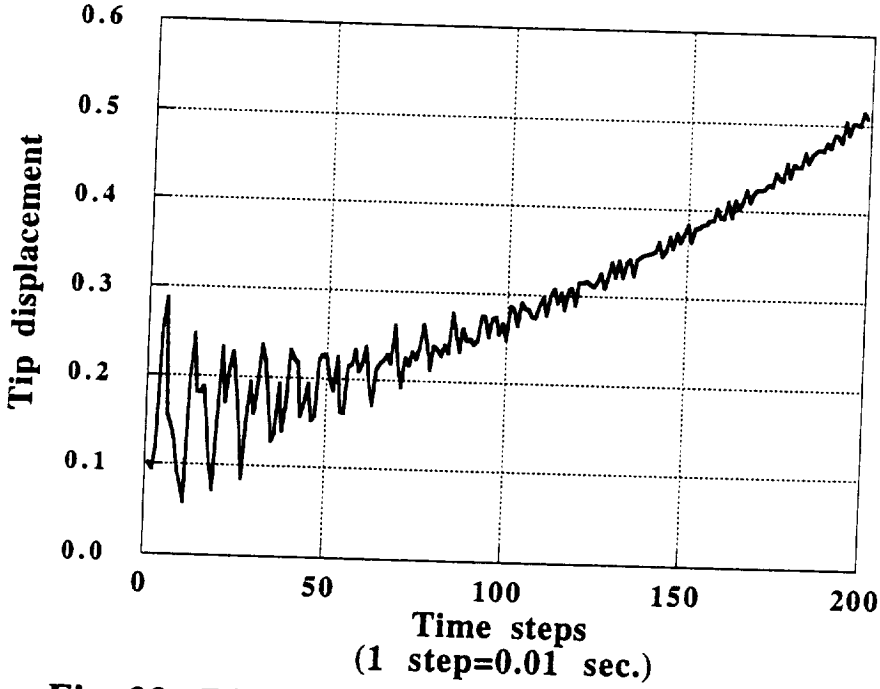

Fig 23. Displacement Vs Time at V=145.0 m/s

(AR=10, Area=20m^2, TR=0.5, Sweep=0^o)

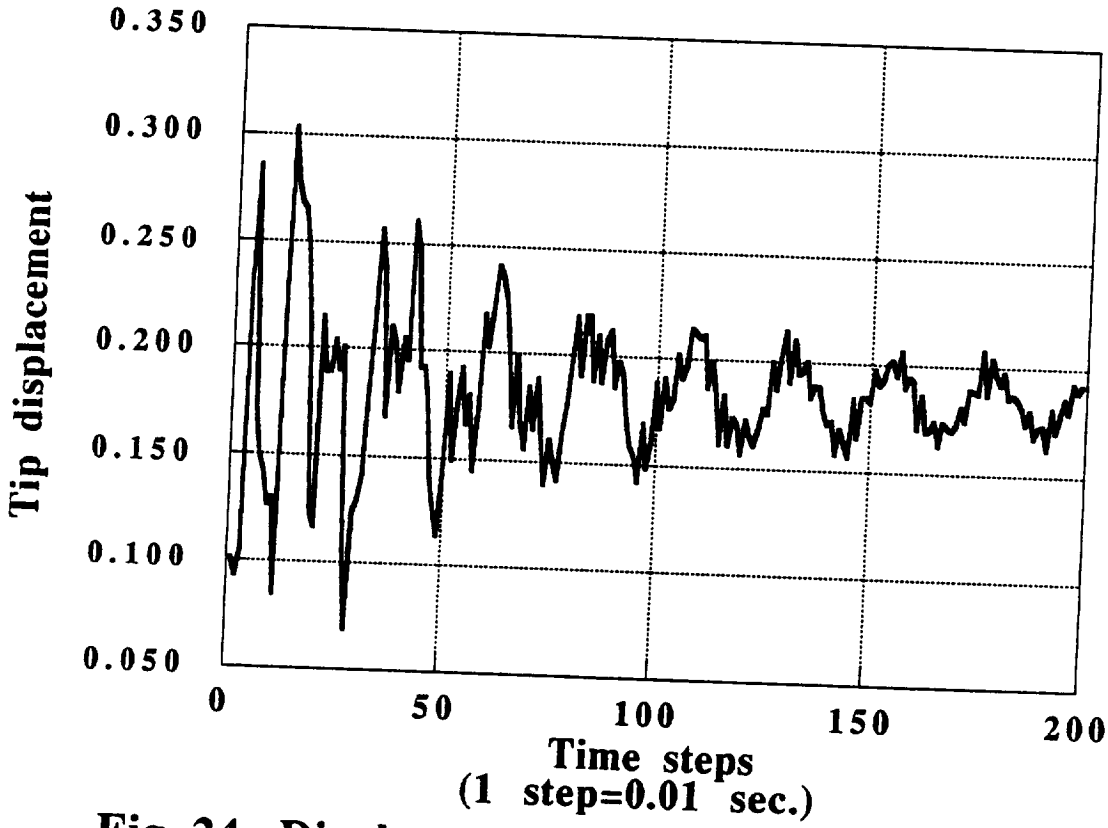

Fig 24. Displacement Vs Time at V=203.74 m/s

(AR=10, Area=20m^2, TR=0.5, Sweep=15^o)

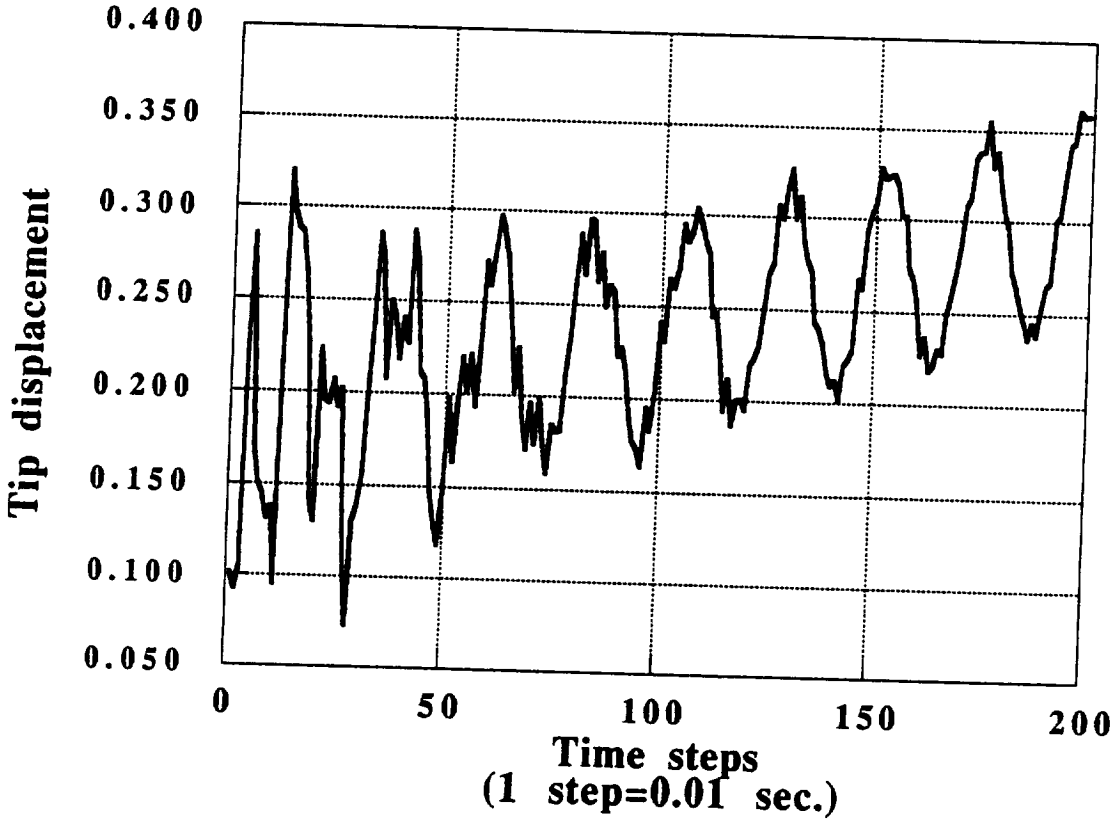

Fig 25. Displacement Vs Time at V=209.67 m/s

(AR=10, Area=20m^2, TR=0.5, Sweep=15^o)

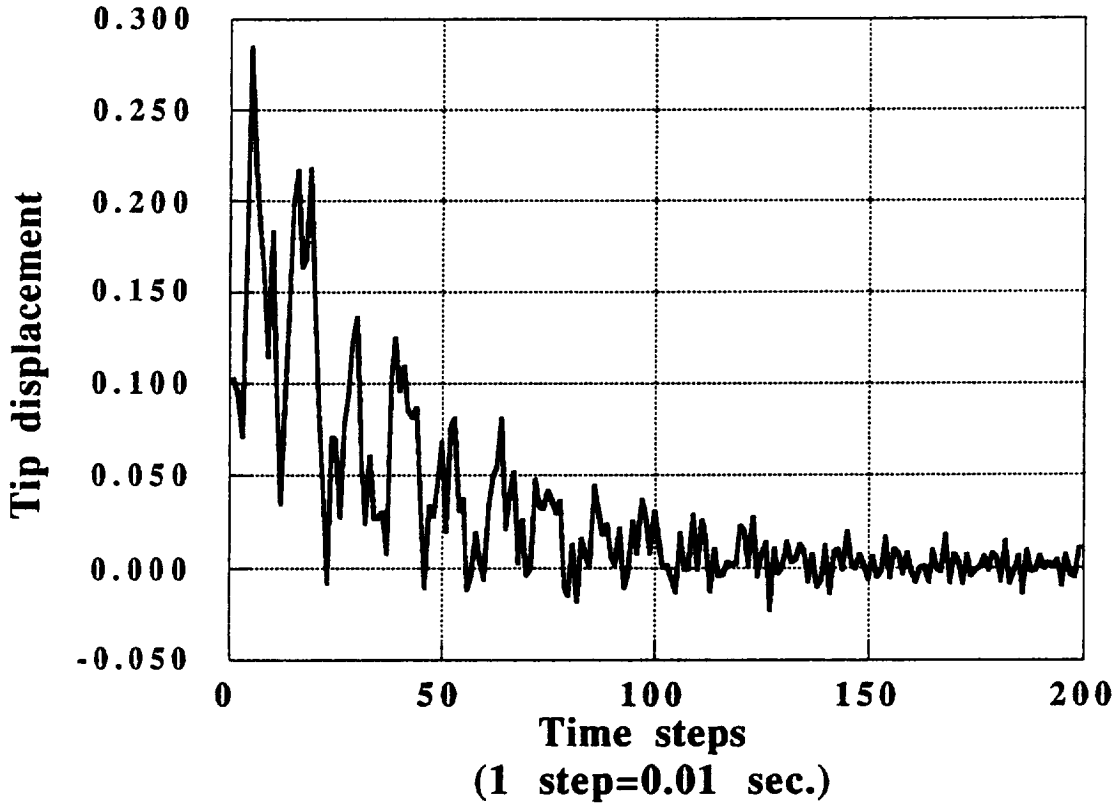

Fig 26. Displacement Vs Time at V=190 m/s

(AR=10, Area=20m^2, TR=0.5, Sweep=30^o)

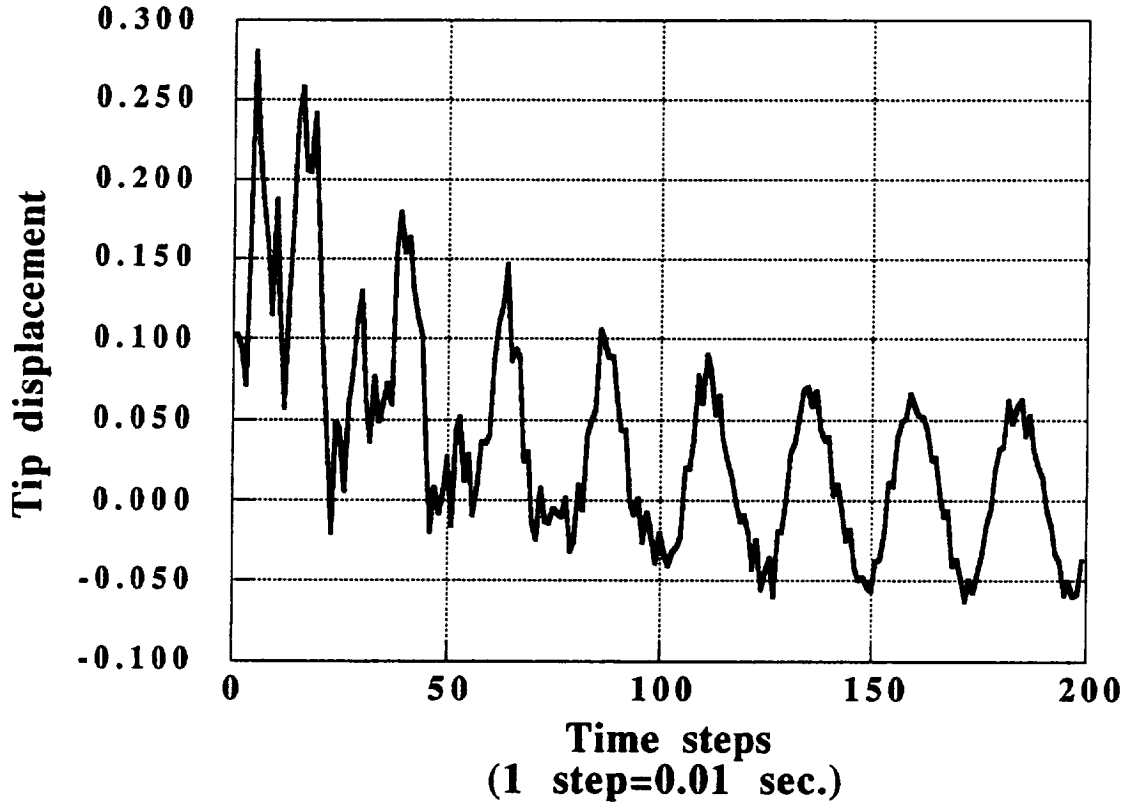

Fig 27. Displacement Vs Time at V=213.22 m/s

(AR=10, Area=20m^2, TR=0.5, Sweep=30^o)

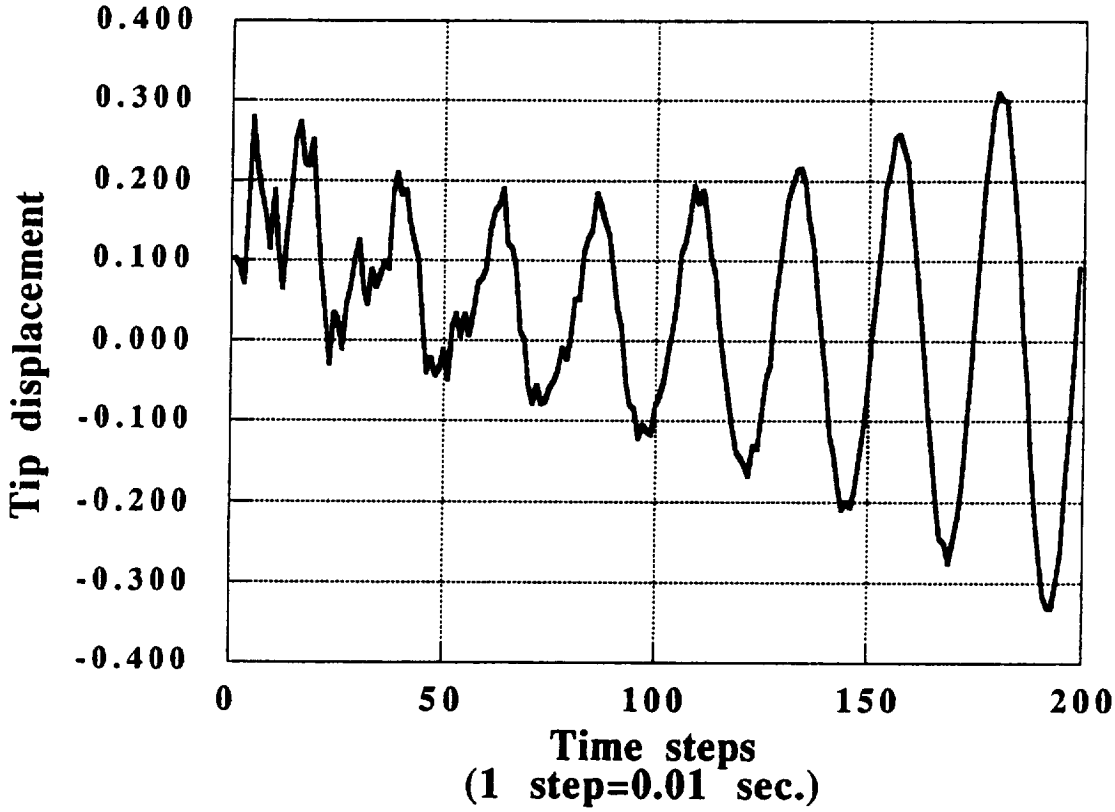

Fig 28. Displacement Vs Time at V=220 m/s

(AR=10, Area=20m^2, TR=0.5, Sweep=30^o)

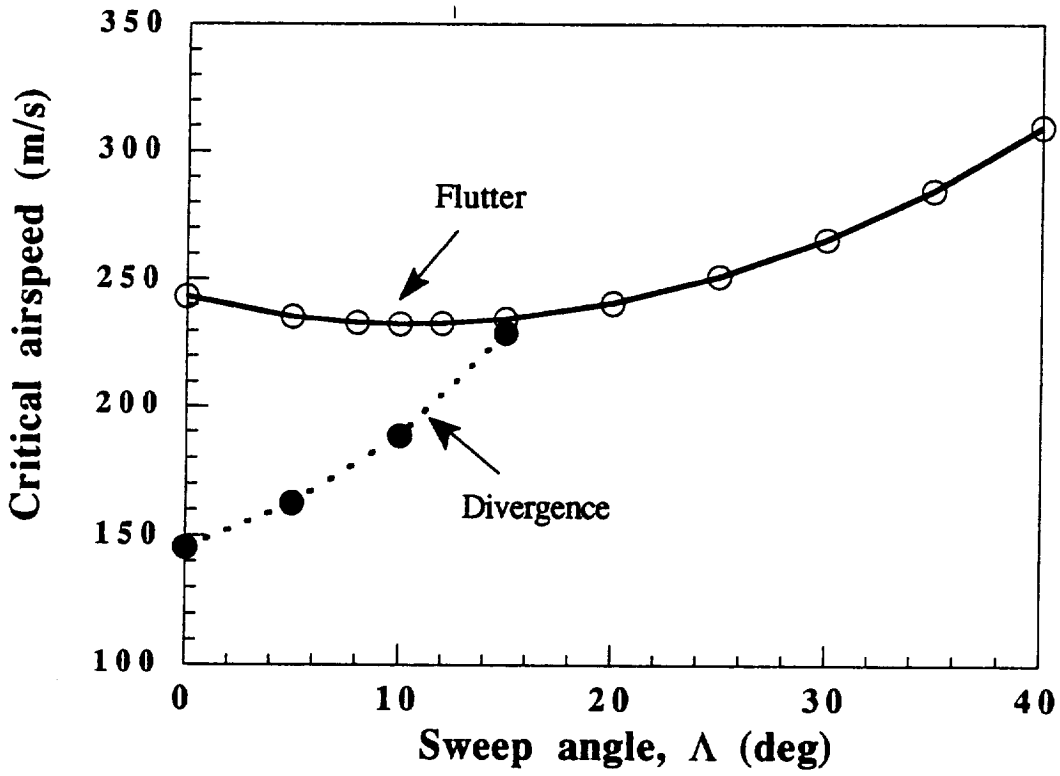

Fig. 29 Critical speed Vs Sweep Angle
(AR=10, Area=20 m^2, TR=0.5)

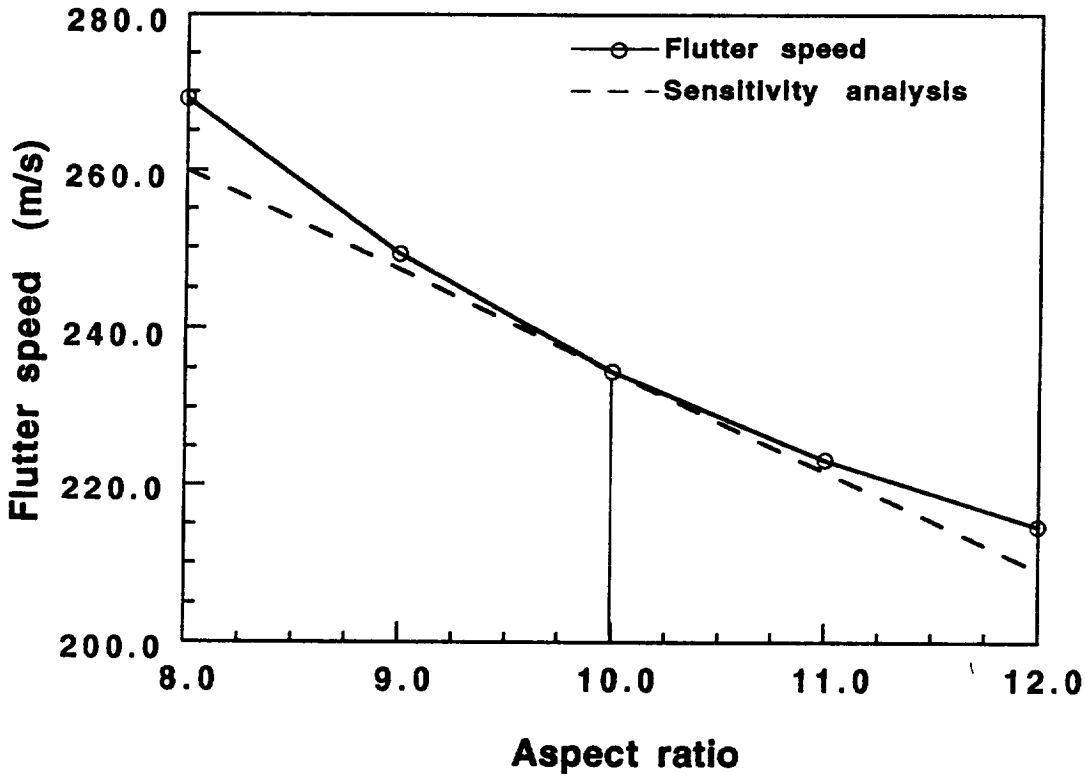

Fig 30. Flutter speed Vs Aspect ratio (M=0.9)

(AR=10, Area=20m^2, TR=0.5, Sweep=15^o)

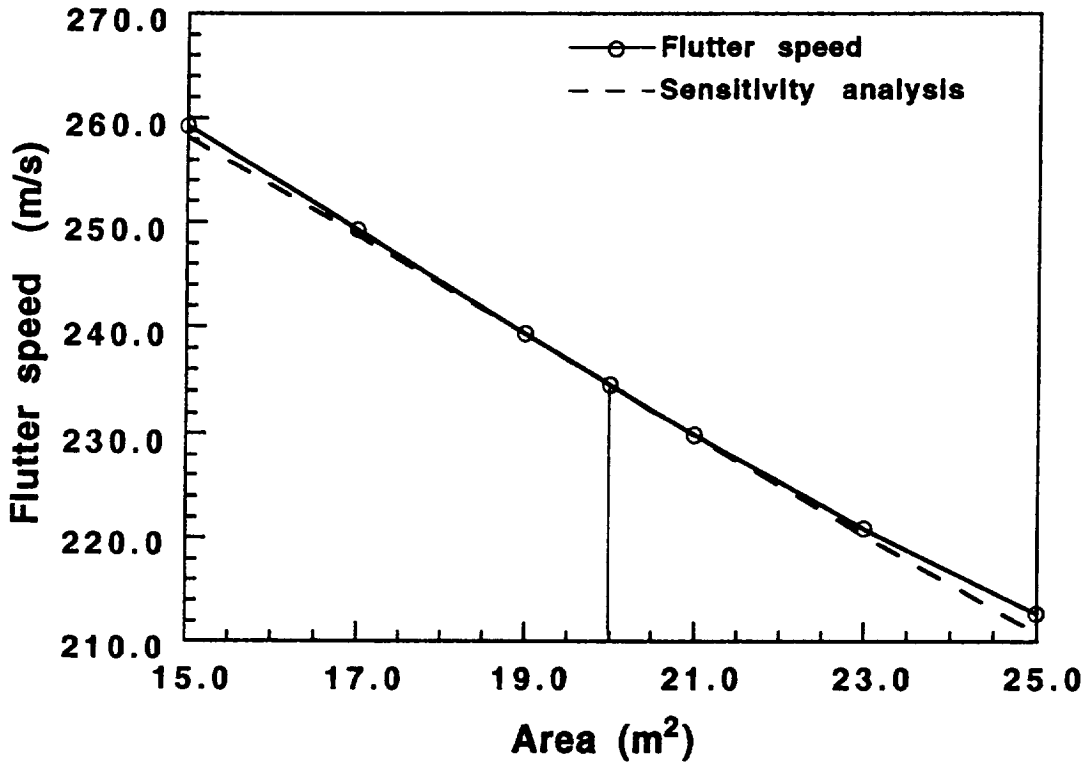

Fig 31. Flutter speed Vs Area (M=0.9)

(AR=10, Area=20m², TR=0.5, Sweep=15°)

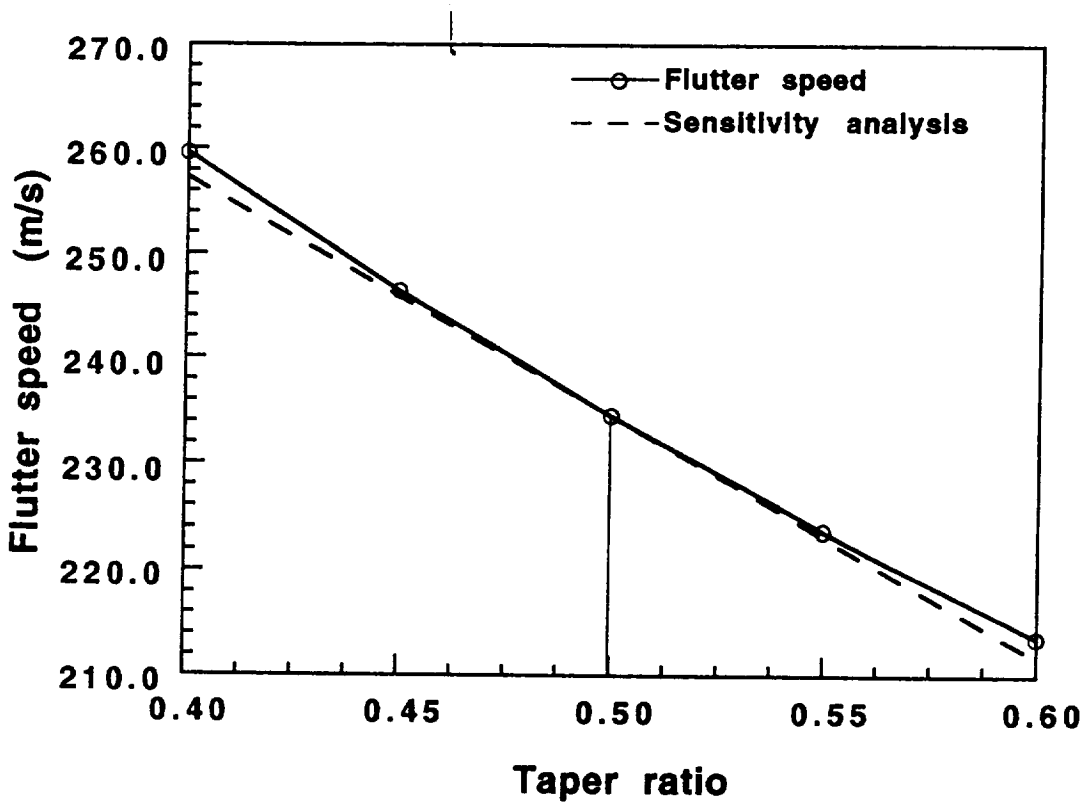

Fig 32. Flutter speed Vs Taper ratio (M=0.9)
(AR=10, Area=20m^2, TR=0.5, Sweep=15^o)

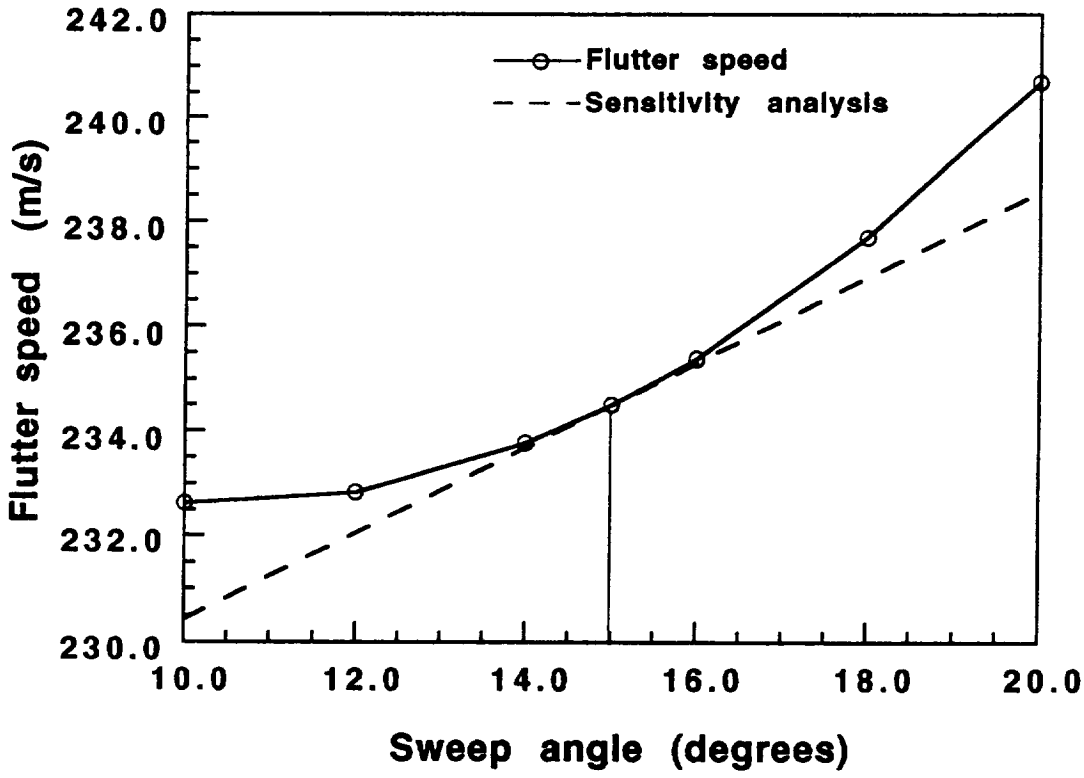

Fig 33. Flutter speed Vs Sweep angle (M=0.9)
(AR=10, Area=20m^2, TR=0.5, Sweep=15^o)